

Review

# Advances in Synthesis and Applications of Single-Atom Catalysts for Metal Oxide-Based Gas Sensors

Yuanting Yu <sup>1</sup> , Yiling Tan <sup>1</sup>, Wen Niu <sup>1</sup>, Shili Zhao <sup>1</sup>, Jiongyue Hao <sup>1</sup>, Yijie Shi <sup>1</sup>, Yingchun Dong <sup>1</sup>, Hangyu Liu <sup>1</sup>, Chun Huang <sup>1</sup>, Chao Gao <sup>1</sup>, Peng Zhang <sup>2</sup>, Yuhong Wu <sup>2</sup>, Linggao Zeng <sup>3</sup>, Bingsheng Du <sup>1,4,\*</sup> and Yong He <sup>1,\*</sup>

<sup>1</sup> Key Laboratory of Optoelectronic Technology and Systems of the Education Ministry of China, College of Optoelectronic Engineering, Chongqing University, Chongqing 400044, China; 202208131049t@stu.cqu.edu.cn (Y.Y.); tan\_yiling@163.com (Y.T.); chevron325@163.com (W.N.); zsl18678631330@163.com (S.Z.); 20230801031@stu.cqu.edu.cn (J.H.); 20172535@cqu.edu.cn (Y.S.); 202208021016@stu.cqu.edu.cn (Y.D.); 202308021039@stu.cqu.edu.cn (H.L.); 20192547@cqu.edu.cn (C.H.); gaoc@cqu.edu.cn (C.G.)

<sup>2</sup> Chongqing Key Laboratory of Toxic and Drug Analysis, Chongqing Police College, Chongqing 401331, China; 13246827609@163.com (P.Z.); d20240677890@163.com (Y.W.)

<sup>3</sup> Chongqing Institute for Food and Drug Control, Chongqing 401121, China; zenglinggao@cqifdc.org.cn

<sup>4</sup> Chongqing Key Laboratory of Optical Fiber Sensor and Photoelectric Detection, Chongqing University of Technology, Chongqing 400054, China

\* Correspondence: bingshengdu@cqu.edu.cn (B.D.); yonghe@cqu.edu.cn (Y.H.)

**Abstract:** As a stable, low-cost, environment-friendly, and gas-sensitive material, semiconductor metal oxides have been widely used for gas sensing. In the past few years, single-atom catalysts (SACs) have gained increasing attention in the field of gas sensing with the advantages of maximized atomic utilization and unique electronic and chemical properties and have successfully been applied to enhance the detection sensitivity and selectivity of metal oxide gas sensors. However, the application of SACs in gas sensors is still in its infancy. Herein, we critically review the recent advances and current status of single-atom catalysts in metal oxide gas sensors, providing some suggestions for the development of this field. The synthesis methods and characterization techniques of SAC-modified metal oxides are summarized. The interactions between SACs and metal oxides are crucial for the stable loading of single-atom catalysts and for improving gas-sensitive performance. Then, the current application progress of various SACs (Au, Pt, Cu, Ni, etc.) in metal oxide gas sensors is introduced. Finally, the challenges and perspectives of SACs in metal oxide gas sensors are presented.

**Keywords:** single-atom catalysts; gas sensor; metal oxide; defect engineering; materials characterization



**Citation:** Yu, Y.; Tan, Y.; Niu, W.; Zhao, S.; Hao, J.; Shi, Y.; Dong, Y.; Liu, H.; Huang, C.; Gao, C.; et al. Advances in Synthesis and Applications of Single-Atom Catalysts for Metal Oxide-Based Gas Sensors. *Materials* **2024**, *17*, 1970. <https://doi.org/10.3390/ma17091970>

Academic Editor: Alben Paskaleva

Received: 8 March 2024

Revised: 2 April 2024

Accepted: 11 April 2024

Published: 24 April 2024



**Copyright:** © 2024 by the authors. Licensee MDPI, Basel, Switzerland. This article is an open access article distributed under the terms and conditions of the Creative Commons Attribution (CC BY) license (<https://creativecommons.org/licenses/by/4.0/>).

## 1. Introduction

Gas sensors are widely used in environmental protection [1–3], healthcare [4–6], food testing [7–10], agricultural production [11–13], and other fields. The development of the Internet of Things (IoTs) puts higher requirements on gas sensors with lower power consumption and higher performance. There are many types of gas sensors, including electrochemical, solid electrolyte, semiconductor, etc. Among them, chemiresistive gas sensors are the most widely used, with the advantages of low cost, good response, and ease of mass production. The core of chemiresistive gas sensors is the sensitive material, and metal oxides are the first commercially available and most researched sensitive materials, with the advantages of low cost, simple structure, and high stability. However, metal oxide-based gas sensors have the disadvantages of high operating temperature and poor selectivity [14].

To facilitate the disadvantages of metal oxide-sensitive materials, defect engineering [15–17], heterogeneous constructing [18–21], noble metal modification [22–24], and various other strategies have been used to improve the gas-sensitive properties of metal oxides. Among them, the strategy of noble metal modification uses the catalytic properties

of noble metals to modify the sensitive materials in such a way that by modulating the adsorption properties and reactivity of gases on the surface of the materials, the enhancement of the selectivity of the sensors can be achieved, as well as the lowering of the operating temperature. For example, Behnam Bahrami et al. doped gold (Au) particles in SnO<sub>2</sub> and investigated its selectivity in a model of a liquefied petroleum gas system (CO, methane, and propane), and they found that the introduction of Au particles improves the selectivity of SnO<sub>2</sub> for CO and reduces the optimal operating temperature [25]. However, these catalysts of different sizes and morphologies will generate multiple active sites, resulting in the actual response of the sensor often being the “superposition effect” of these multiple catalytic effects, which results in a response to different types of gases and a decrease in their selectivity.

Single-atom catalysts are isolated single atoms dispersed on supports without any form of interaction between each individual atom [26–28]. It has been found that when doping or modifying the support material using single atoms, on the one hand, due to strong metal–support interactions, it promotes charge redistribution at the interface, which makes the support interface around the single atoms more active and more likely to adsorb gas molecules and promotes the chemical reaction at the gas/solid interface to increase the reactivity [29,30]. On the other hand, unlike heterogeneous catalysis produced by nano-catalysts, due to the single active site of single atoms, each active center will produce the same geometry, which will avoid the atomistic catalytic pathway, reduce the side reactions, and improve the reaction selectivity [31]. For example, Georgios Kyriakou’s group found that a single isolated Pd atom on the copper surface greatly reduces the energy barrier for hydrogen absorption and subsequent desorption on the copper metal surface and that hydrogen dissociation at the Pd atomic site and weak binding to copper resulted in excellent selectivity for the hydrogenation of styrene and acetylene compared to pure copper or palladium metal [32]. Based on those advantages of SACs, it has been successfully applied to make up for the shortcomings of metal oxide-sensitive materials. In recent years, the noble metal single-atom catalysts of Pt, Pd, Au, etc., have been commonly used for decorating the metal oxide gas sensing materials of SnO<sub>2</sub>, WO<sub>3</sub>, ZnO, and In<sub>2</sub>O<sub>3</sub> to improve the response and selectivity or reduce the operation temperature.

However, research on the gas-sensitive properties of metal oxide-loaded SACs is still in its infancy [33,34]. There are some limitations that restrict its development, such as the limited synthesis and characterization methods, agglomeration and growth up of catalysts, and the unclear relationship between sensing performance and the catalysts. Thus, it is necessary to summarize the current synthesis and characterization methods, stabilization strategies, and the gas sensing properties in order to gain an insightful understanding of their development direction. In this review, we take the research progress of single-atom catalyst-functionalized metal oxide gas sensors as a starting point and systematically outline the synthesis and characterization methods of SACs, the interactions between SACs and metal oxide supports, as well as the related gas sensing performance studies. Finally, the challenges and perspectives of SACs in the application of metal oxide-based gas-sensitive materials are presented.

## 2. Synthesis Methods of SAC-Functionalized Metal Oxides

The synthesis of metal oxides loaded with SACs is a prerequisite for studying their structural features and exploring their applications. Achieving the monodisperse without the agglomeration of single-atom catalyst-modified metal oxides is the goal of exploring the synthesis strategies. Currently, the common strategies for loading SACs on metal oxides include atomic layer deposition, impregnation, co-precipitation, photochemistry, and space-limiting strategies. Next, we summarize several typical methods of SACs synthesis.

### 2.1. Atomic Layer Deposition (ALD)

Atomic layer deposition is a thin-film deposition technique based on a self-limiting surface reaction with high homogeneity. It is a technique that can be precisely controlled at

the atomic level [35–37]. Numerous studies have been conducted to design and successfully synthesize SAC-loaded materials by the ALD method. The study of metal oxides as supports and loading SACs on their surfaces by ALD has been applied in the fields of CO oxidation, oxygen precipitation catalysis, gas sensing, etc. Zhao et al. succeeded in uniformly depositing Ru single atoms on the surface of  $\text{Co}_3\text{O}_4$  by ALD, and the as-made Ru single atom served as a catalyst for the oxygen precipitation reaction, as shown in Figure 1a. The catalytic activity was increased to 95.5 times compared with that of pure  $\text{Co}_3\text{O}_4$ . Theoretical calculations showed that the Ru single atom acts as a promoter and improves the catalytic activity by modulating the binding energy between the intermediate and the active site [38]. Wang et al. reported a general ALD strategy with uniformly dispersed Fe single atoms loaded up to 1.78 wt% on multiwalled carbon nanotubes,  $\text{SiO}_2$ , and  $\text{TiO}_2$  substrates, and the reaction scheme is shown in Figure 1b. Among them, the Fe/ $\text{TiO}_2$  system was used for the catalytic degradation of a methylene blue (MB) solution. Experimental investigations showed that the photocatalytic activity of  $\text{TiO}_2$  obtained after two Fe ALD cycle depositions was about six times higher than that of pure  $\text{TiO}_2$  [39]. Figure 1c illustrates the flowchart for the deposition of single-atom Pt on graphene. The Pt precursor first reacts with adsorbed oxygen ( $\text{O}^*$ ) on the graphene surface, and then the Pt precursor is converted to Pt-O species by oxygen pulses to form a new adsorbed oxygen layer on the Pt surface. The single-atom-loaded catalysts prepared by the ALD method showed excellent advantages, but clusters were easily formed because the metal atoms deposited by ALD preferred to be adsorbed on the existing metal atoms. Moreover, ALD technology is complicated to operate and requires expensive equipment, which limits its large-scale production application [40]. 5

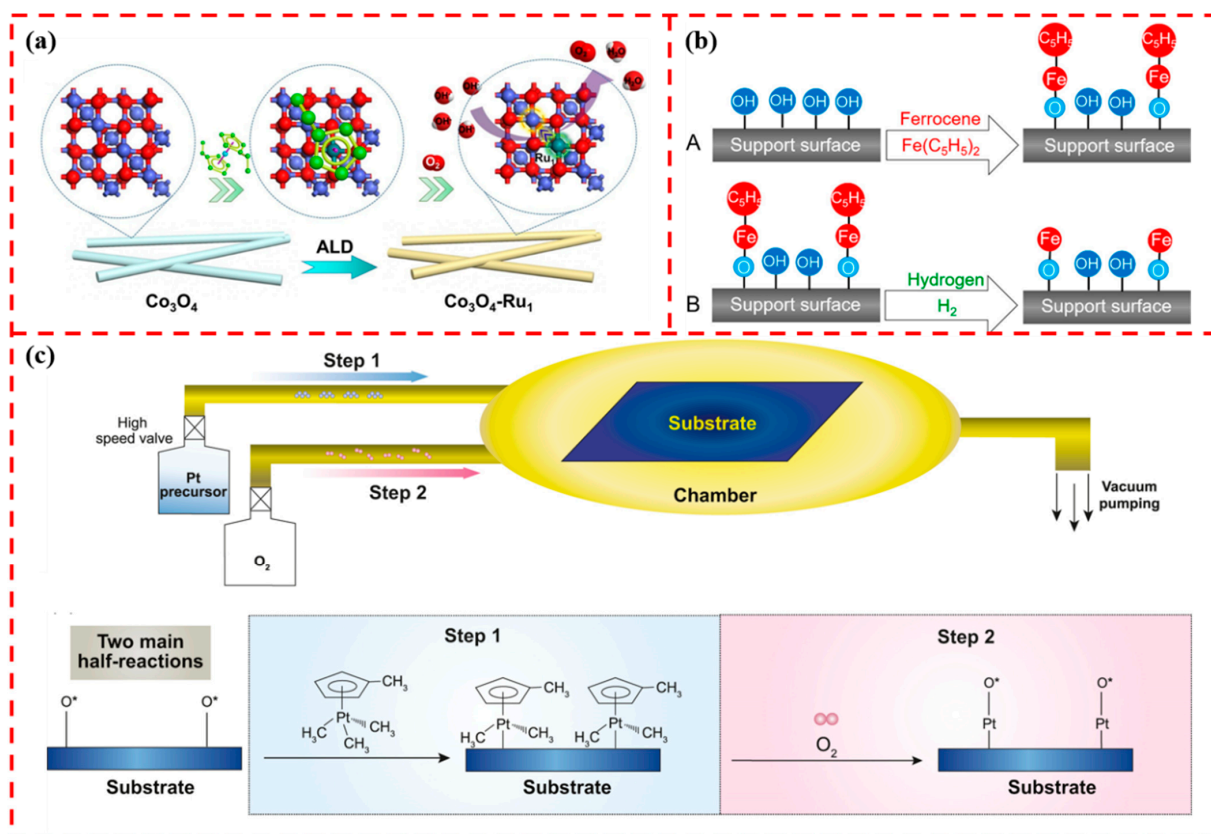


**Figure 1.** (a) Schematic representation of single-atom Ru loading on  $\text{Co}_3\text{O}_4$  by ALD. Reprinted with permission from Ref. [38]. Copyright 2020, Elsevier. (b) Reaction scheme of the Fe-ALD half-reaction. Reprinted with permission from Ref. [39]. Copyright 2020, American Chemical Society. (c) Schematic representation of the deposition of Pt single atom and the two main half-reactions on a support by ALD. Reprinted with permission from Ref. [40]. Copyright 2018, Science Press.

## 2.2. Impregnation

The impregnation method first adsorbs the metal precursor on the surface of the support and then thermally decomposes the metal precursor by annealing and removing the ligand while enhancing the interaction of the single atoms with the support. Compared with the ALD method, the impregnation method has the advantages of simple operation and low cost and is widely used in industry for loading metal catalysts [41,42]. Zhang et al. successfully loaded atomically dispersed Pt on RuO<sub>2</sub> by impregnation and confirmed the random presence of Pt single atoms on the surface of RuO<sub>2</sub> by high-angle annular dark-field (HAADF). The catalytic activity of Pt<sub>1</sub>/RuO<sub>2</sub> for methanol oxidation was investigated and found to be 15.3 times higher than that of the commercial catalyst Pt/C. Pt<sub>1</sub>/RuO<sub>2</sub> also exhibited excellent catalytic stability [43].

The high surface free energy of single atoms makes them susceptible to migration and agglomeration, generating nanoclusters or nanoparticles with low surface energy [44]. The preparation of SACs by the impregnation method suffers from the disadvantages of low loading and non-uniform dispersion. Thus, it is necessary to inhibit atomic aggregation while increasing the single-atom loading rate. Hai et al. prepared SACs by combining impregnation method with the two-step annealing method, which is schematically shown in Figure 2a. Fifteen kinds of metals were successfully loaded on NC, PCN, and CeO<sub>2</sub> supports with the highest loading of 23 wt% (Figure 2b), which greatly improved the single-atom loading rate and also provided an avenue for exploring the library of monometallic/multimetallc catalysts [45]. This is a novel extension of the impregnation method and demonstrates the potential of the impregnation method in achieving high SACs loads.

## 2.3. Coprecipitation and Hydrothermal

Coprecipitation is a typical method for the preparation of metal catalysts. In this method, uniformly loaded metal catalysts are prepared by using metal ions as precursors and adding a precipitant to an aqueous solution of the precursor to produce a precipitate [46]. Wei et al. obtained Pt single-atom-loaded FeO<sub>x</sub> catalysts by coprecipitation using a chloroplatinic acid (H<sub>2</sub>PtCl<sub>6</sub>·6H<sub>2</sub>O) precursor and iron nitrate (Fe(NO<sub>3</sub>)<sub>3</sub>·9H<sub>2</sub>O) aqueous solution. Due to the strong interaction between the Pt single atom and the FeO<sub>x</sub> support, the catalyst acted for the hydrogenation of 3-nitrostyrene at a TOF of ~1500 h<sup>-1</sup>, with a selectivity of close to 99% for 3-aminostyrene, demonstrating excellent catalytic performance [31]. Millet et al. synthesized a series of Ni<sub>x</sub>Mg<sub>1-x</sub>O samples with different Ni concentrations (0–15 at%) by coprecipitation. Among them, the STEM-HAADF images of the samples with a Ni concentration of 10% are shown in Figure 2c. The Ni single-atom sites are marked with a red circle in Figure 2d, which serve as the active sites for CO<sub>2</sub> activation [47].

Similarly, the hydrothermal method was adopted to synthesize SACs by adding the metal ions and salt solution to a stainless-steel autoclave reactor. For example, Shah et al. obtained Co-incorporated RuO<sub>2</sub> catalysts by a one-pot hydrothermal process followed by calcination. The Co single atom not only greatly alleviated the stability problems of RuO<sub>2</sub> under alkaline OER conditions but also substantially elevated the HER activity of Ru-based electrocatalysts under acidic HER conditions. [48]. Gu et al., through the modified hydrothermal method, prepared an Fe single-atom-decorated MnO<sub>2</sub>, which exhibited a stronger O<sub>2</sub> activation performance than the conventional surface oxygen vacancy activation sites [49].

The coprecipitation and hydrothermal methods have certain disadvantages: the metal precursor and the support precursor are precipitated at the same time, and the metal catalyst will inevitably be embedded in the body material of the support, resulting in a certain degree of waste. However, coprecipitation and hydrothermal methods are easy to operate, low cost, and suitable for large-scale production [46]. At present, the application of the coprecipitation and hydrothermal methods for loading SACs occurs less often than that

of the impregnation method in the wet chemical method, and it is worthwhile to further explore the application of this method.

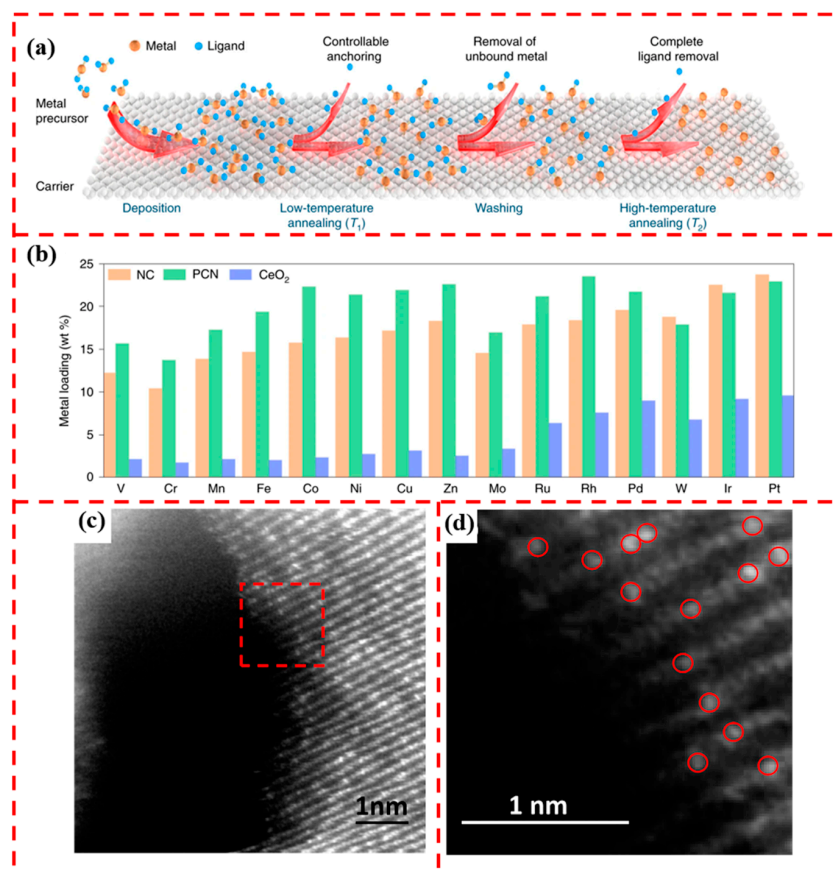


**Figure 2.** (a) Two-step annealing strategy for loading single atoms. (b) Metal loading achieved on NC, PCN, and CeO<sub>2</sub> supports. Reprinted with permission from Ref. [45]. Copyright 2022, Springer Nature. (c) STEM-HAADF image of the Ni<sub>x</sub>Mg<sub>1-x</sub>O sample with Ni concentration of 10%. (d) Magnified image of the selected region of the red dotted square in (c), with Ni single atoms circled in red. Reprinted with permission from Ref. [47]. Copyright 2019, American Chemical Society.

#### 2.4. Photochemical Method

The photochemical method does not require high-temperature pyrolysis compared to impregnation and coprecipitation. It is a mild method of loading SACs [50]. Liu et al. synthesized single-atom Pd-loaded TiO<sub>2</sub> nanosheets via a photochemical route. TiO<sub>2</sub> is inherently photoactive, and under UV irradiation, EG radicals are generated on the surface of TiO<sub>2</sub>. The presence of EG radicals helps in the removal of Cl<sup>-</sup> from the Pd precursor ions, leaving Pd single atoms on the surface. In the hydrogenation of C=C bonds, the Pd<sub>1</sub>/TiO<sub>2</sub> catalyst exhibits nine times higher catalytic activity than commercial Pd catalysts with excellent stability [51].

Wei et al. obtained atomically dispersed platinum by irradiating frozen chloroplatinic acid solutions with UV light. The ice lattice naturally restricts the migration and agglomeration of the atoms, and a flow chart of the method is shown in Figure 3a. Aberration-corrected high-angle annular dark-field scanning transmission electron microscopy (HAADF-STEM) characterization result plots confirm the successful loading of Pt single atoms. This method was applied to successfully loaded platinum single atoms on different supports such as mesoporous carbon, graphene, carbon nanotubes, titanium dioxide nanoparticles, and zinc oxide nanowires. The combination of low temperature and photochemistry is confirmed to be an effective method for loading single-atom catalysts. The photochemical method requires mild reaction conditions and has potential applications in the field of sustainable

energy and green chemistry, contributing to the environmental friendliness of catalytic reactions [52].

### 2.5. Space Limitation Strategy

It is well known that metal–organic framework (MOF) materials are regularly porous. This feature facilitates the adsorption and anchoring of metal precursors, prevents agglomeration, and is more conducive to the successful synthesis of SACs [53]. MOFs can be pyrolyzed at high temperatures to obtain a series of derivatives of MOFs, such as nitrogen-doped porous carbon, metal oxides, etc., which tend to retain the porous characteristics of MOFs. Therefore, the spatial confinement of single atoms through MOF porous templates and subsequent high-temperature annealing steps to obtain single-atom-loaded MOF derivative materials is an effective strategy for loading SACs.

Currently, most studies focus on MOF-derived porous nitrogen-doped carbon materials loaded with SACs [54,55] and relatively few studies have been carried out on MOF-derived oxides loaded with single-atom metal catalysts. Liu et al. used In-MOF as a template, loaded with Pd single atoms, and after high-temperature pyrolysis treatment, Pd single-atom-modified  $\text{In}_2\text{O}_3$  was obtained, and the preparation process is schematically shown in Figure 3b [56]. By varying the introduction amount of Pd precursor ions, Pd single-atom-loaded, PdO cluster-loaded  $\text{In}_2\text{O}_3$  were synthesized. By annealing under a reducing atmosphere, Pd nanoparticle-loaded  $\text{In}_2\text{O}_3$  was obtained.  $\text{H}_2\text{S}$  gas was detected using the above three materials, in which the Pd single-atom-loaded  $\text{In}_2\text{O}_3$  showed the optimal detection ability under the same testing conditions. This is attributed to the high uniformity of the loaded Pd single-atom sites, which greatly improves the surface adsorption energy for  $\text{H}_2\text{S}$  gas. The study on MOF-derived oxides loaded with SACs deserves further investigation.

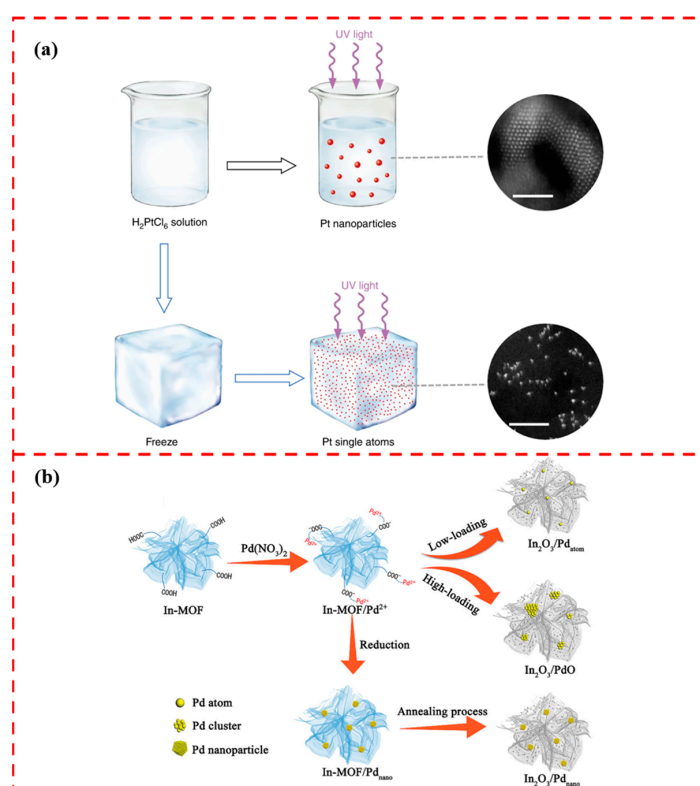


**Figure 3.** (a) Schematic diagram of cryo-photochemically loaded Pt single-atom catalyst. Reprinted with permission from Ref. [50]. Copyright 2017, Springer Nature. (b) Schematic diagram of In-MOF as a template for loading single-atom Pd. Reprinted with permission from Ref. [56]. Copyright 2021, John Wiley and Sons.

### 3. Characterization of SAC-Functionalized Metal Oxides

The successful loading of SACs on metal oxides needs to be demonstrated by corresponding material characterization techniques. Here, we summarize several typical characterization techniques that can directly prove the stable loading of SACs. These techniques can be divided into two main categories according to their results: (1) Morphological characterization: mainly including high-resolution high-angle annular dark-field scanning transmission electron microscopy (HAADF-STEM) and scanning tunneling microscopy (STM). (2) Structural information characterization: X-ray photoelectron spectroscopy, extended X-ray absorption fine structure, X-ray absorption near-edge structure, and Fourier-transform infrared spectroscopy.

#### 3.1. HAADF-STEM and STM

HAADF-STEM is a transmission electron microscopy technique that allows images with atomic-level resolution to be obtained by measuring the high-angle scattering of transmitted electrons in a sample. Compared to conventional TEM, the contrast of HAADF-STEM images correlates with atomic number, and the atoms of heavier elements produce more scattering than lighter elements, appearing brighter in the image, which can significantly improve the detection sensitivity at sizes below 1 nm. HAADF-STEM can provide the most intuitive evidence for the successful loading of SACs [57,58]. As shown in Figure 4a, which is the TEM image of  $\text{CoO}_x$  loaded with single-atom Ru, it can be observed that the initial morphology of  $\text{CoO}_x$  does not change after the introduction of single-atom Ru. EDS mapping confirmed that the Ru element was uniformly distributed in  $\text{CoO}_x$  nanosheets. Through HAADF-STEM images, some bright spots on the surface of  $\text{CoO}_x$  can be observed, which is atomically dispersed Ru, highlighted by orange circles in the Figure 4a [59]. In Figure 4b, several atom-sized bright spots (highlighted with yellow circles) can be clearly observed, which are attributed to the presence of Au single atoms in the  $\text{Au}_{0.1}\text{Ag}_{0.9}$  alloy NPs. Figure 4c shows the intensity distribution of the labelled regions in Figure 4b, further confirming the atomic dispersion of Au in the  $\text{Au}_{0.1}\text{Ag}_{0.9}$  alloy NPs [60].

STM is a scanning probe microscopy technique with atomic-level resolution, but because it cannot transmit the sample, it can only provide information about the sample surface. However, it also makes up for the shortcomings of HAADF-STEM in which the electron beam may cause electron radiation damage to the sample. Figure 4d shows the STM image of the Pt/Cu monoatomic alloy, and it can be clearly observed that in the Pt/Cu monoatomic alloys (SAAs), the Pt atoms are able to alloy directly into the area near the steps and step edges and are randomly distributed over the entire surface [61].

#### 3.2. XANES and EXAFS

The isolated presence of single atoms can be visualized by HAADF-STEM and STM technique characterization, but the help of spectroscopic analysis techniques is required to further analyze the detailed chemical information of single atoms. X-ray absorption spectroscopy (XAS) plays an important role in probing the electronic structure, geometry, coordination environment, and other information of atoms. According to the division of energy spectra in different regions, the XAS technique can be divided into X-ray near-edge absorption fine structure spectroscopy (XANES) and X-ray extended-edge absorption fine structure (EXAFS). XANES measures the region from  $-50$  to  $150$  eV away from the absorption edge, which is associated with the jump of electrons from the inner shell to valence orbitals. EXAFS measures the energy range from  $150$  to  $1000$  eV, and the local environment of the atoms in the material is obtained by analyzing the structure of oscillations away from the absorption edge in the X-ray absorption spectra. These characterization techniques can provide information about interatomic distances, coordination numbers, and atom types [62]. The application of XANES and EXAFS techniques can provide a more comprehensive understanding of the atomic structure of single-atom catalysts [63].

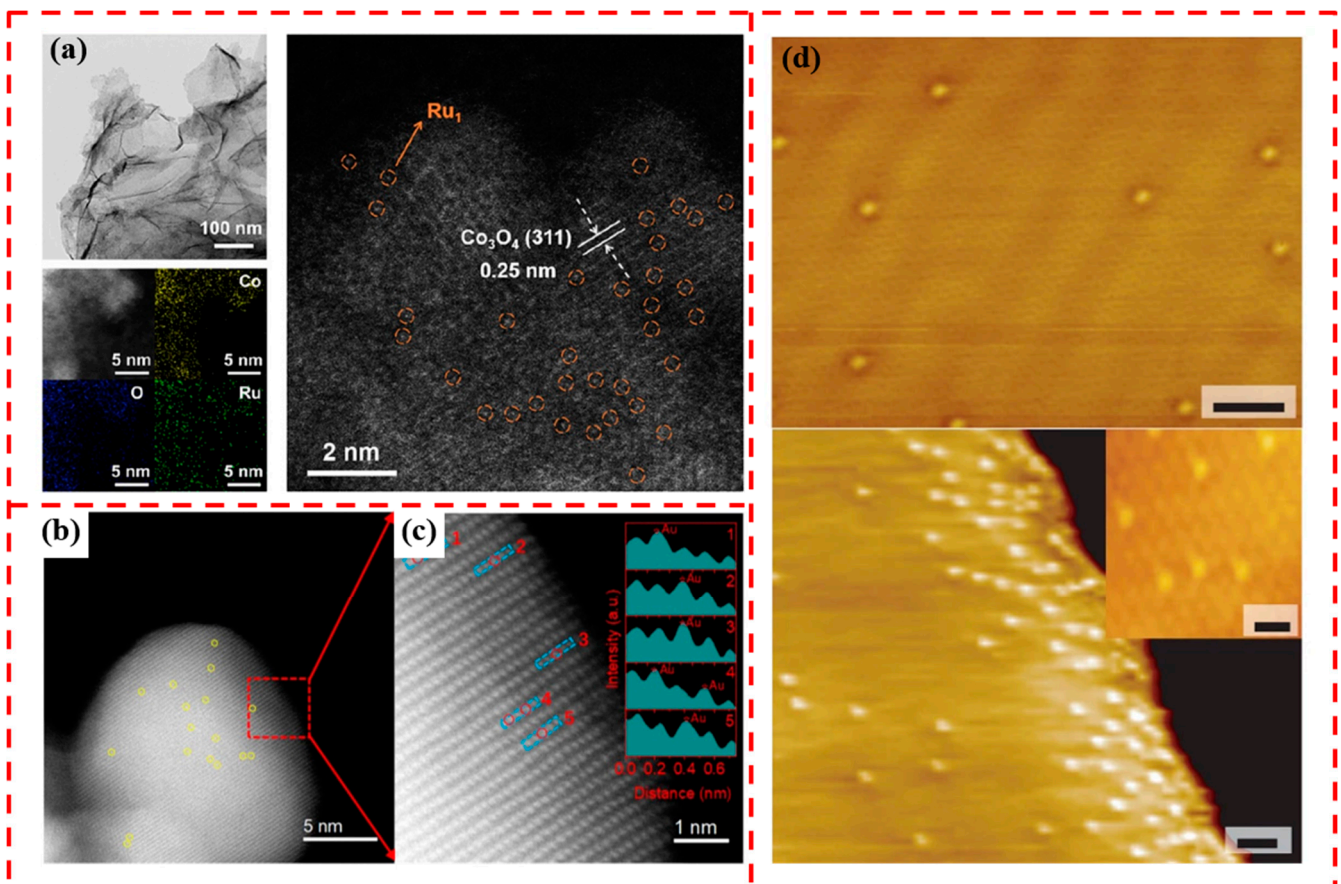


**Figure 4.** (a) TEM image of Ru<sub>1</sub>/CoO<sub>x</sub>, aberration-corrected HAADF-STEM EDS image and HAADF-STEM image of aberration-corrected Ru<sub>1</sub>/CoO<sub>x</sub>, where orange circles highlight monodisperse Ru atoms. Reprinted with permission from Ref. [59]. Copyright 2023, American Chemical Society. (b) High-resolution AC-HAADF-STEM image of Au<sub>0.1</sub>Ag<sub>0.9</sub>-ZnO. (c) Enlarged high-resolution AC-HAADF-STEM image of Au<sub>0.1</sub>Ag<sub>0.9</sub>-ZnO and the corresponding intensity profiles at the labelled positions. Reprinted with permission from Ref. [60]. Copyright 2023, John Wiley and Sons. (d) STM image of 0.01 ML Pt/Cu(111) SAA surface. Reprinted with permission from Ref. [61]. Copyright 2018, Springer Nature.

Xu et al. performed XANES and EXAFS analyses in order to investigate the chemical state and coordination environment of single-atom Pt in anchored non-porous TiO<sub>2</sub> and obtained the spectra shown in Figure 5a. In Figure 5a, the intensity of the white line reflecting the oxidation state of Pt is between Pt foil and PtO<sub>2</sub>, indicating that the valence state of Pt in the sample is between 0 and +4. In the R-space FT-EXAFS spectrum, only a prominent peak centered on the Pt-O contribution is observed at 1.68 Å, and almost no Pt-Pt contribution is observed, suggesting that only single Pt atoms are anchored in the non-porous TiO<sub>2</sub>, and no Pt nanoparticles are present [64]. Huang et al. prepared atomically dispersed Ag on polyhedral Co<sub>3</sub>O<sub>4</sub> surfaces by top-down approach. The white line intensity of the samples obtained from Ag-L3-XANES measurements was compared with the standards. As shown in Figure 5b, the near-edge spectrum of the Ag/Co<sub>3</sub>O<sub>4</sub>-polyhedron fresh sample is very similar to that of Ag metal. For metallic Ag, the white line adsorption at about 3355 eV is relatively weak, and it can be determined that the Ag in the sample is mainly in a non-metallic state. In contrast, the white line intensity of the Ag<sub>1</sub>/Co<sub>3</sub>O<sub>4</sub>-polyhedron sample is similar to that of Ag<sub>2</sub>SO<sub>4</sub>, indicating that Ag cations dominate in the thermally aged sample. Figure 5c shows the Ag K-edge extended XAFS (EXAFS) analysis of Ag<sub>1</sub>/Co<sub>3</sub>O<sub>4</sub> and Ag/Co<sub>3</sub>O<sub>4</sub>. The Ag-Kedge spectra of Ag/Co<sub>3</sub>O<sub>4</sub> polyhedron samples and the Ag-Kedge spectra of Ag foils are not significantly different

except for the decrease in amplitude, which suggests that the Ag atoms in the Ag/Co<sub>3</sub>O<sub>4</sub> polyhedron sample are mainly retained in the metal. The Ag atoms of the polyhedral samples are mainly retained the original Ag lattice of the metal particles. After calcination at 250 °C, another tunable peak can be seen in the EXAFS in the 1 to 2 Å region of the Ag<sub>1</sub>/Co<sub>3</sub>O<sub>4</sub> polyhedron, which is attached to Ag-O. This indicates that the surface Ag atoms are oxidized in agreement with the XANES findings. Fitting the EXAFS data to this region, as shown in Figure 5c, yields atomically dispersed Ag cations with three Ag-O bonds [65].

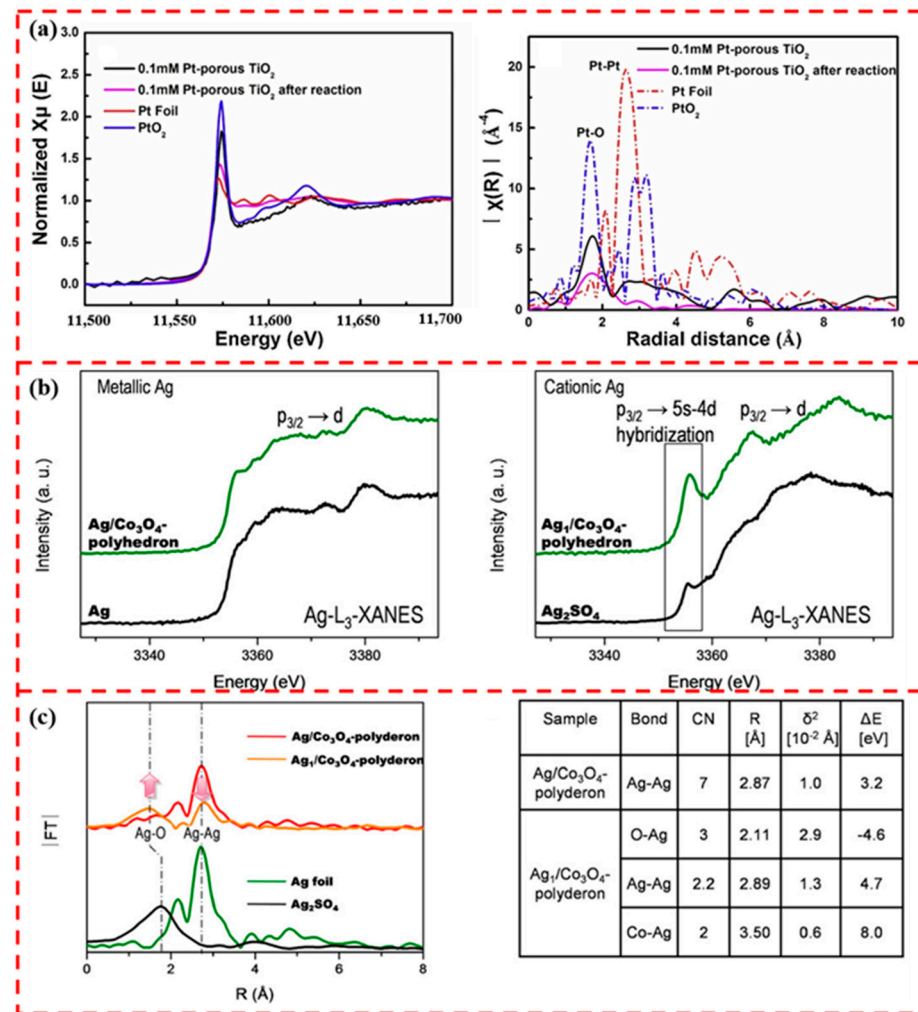


**Figure 5.** (a) Pt L3-edge XANES, and R-space FT-EXAFS spectra. Reprinted with permission from Ref. [64]. Copyright 2019, Elsevier. (b) Ag L3-edge XANES spectra of Ag/Co<sub>3</sub>O<sub>4</sub> polyhedral samples, Ag foil standards, Ag<sub>1</sub>/Co<sub>3</sub>O<sub>4</sub> polyhedral samples, Ag<sub>2</sub>SO<sub>4</sub> Ag L3 edge XANES spectra of polyhedral samples and Ag foil standards. (c) Fourier transform of EXAFS spectra of Ag<sub>1</sub>/Co<sub>3</sub>O<sub>4</sub> polyhedron, Ag<sub>1</sub>/Co<sub>3</sub>O<sub>4</sub> polyhedron with respect to Ag foil and Ag<sub>2</sub>SO<sub>4</sub>, and results of the fitting of Ag-K edge EXAFS data. Reprinted with permission from Ref. [65]. Copyright 2020, Wiley-VCH Verlag GmbH & CO. KGaA.

### 3.3. FT-IR

Different molecules can absorb infrared radiation in a specific range, causing the chemical bonds within the molecules to vibrate, rotate, or stretch, resulting in a specific vibrational frequency. Infrared spectroscopy techniques can be used to analyze and identify compounds based on this principle. Infrared techniques are widely used in the characterization of catalysts due to their excellent sensitivity and the affordability of the equipment [66,67]. Infrared spectroscopy can indirectly obtain molecular information by

tracking the adsorption of the probe molecule on the catalyst surface. Using CO as the probe molecule, the frequency shift of the C–O vibration can be analyzed to obtain the metal type, adsorption site, and other related information at the atomic level, which can provide rich information about the structure of the SACs [68–70]. Fourier-transform infrared spectroscopy (FT-IR) is an effective technique for the characterization of SACs, which uses the Fourier-transform technique to simultaneously acquire information over the entire infrared spectral range. This improves the speed of data acquisition and signal-to-noise ratio compared to conventional dispersive infrared spectrometers.

Qiao et al. prepared FeO<sub>x</sub> with a Pt loading of 0.17 wt% and FeO<sub>x</sub> with a Pt loading of 2.5 wt%, which are noted as Sample A and Sample B, respectively. The FT-IR spectra of the two samples are shown in Figure 6a,b, respectively [71]. In the in situ FT-IR spectrum of sample A, CO adsorption shows only one weak band at 2080 cm<sup>-1</sup>, which is attributed to Pt<sup>δ+</sup>. In the in situ FT-IR spectrum of sample B, a strong vibrational and two weak vibrational bands are generated at 2030 cm<sup>-1</sup>, 1860 cm<sup>-1</sup>, and 1950 cm<sup>-1</sup>, respectively. The strong vibrational band at 2030 cm<sup>-1</sup> is attributed to the linear bonding of the CO on the Pt<sup>0</sup> site. The bands at 1860 cm<sup>-1</sup> and 1950 cm<sup>-1</sup> are generated at two Pt atoms bridging adsorbed CO and adsorbed CO at the direct interface between the Pt cluster and the carrier. Different to Figure 6b, the energy band positions of CO adsorbed in sample A in Figure 6a hardly change with the increase in CO pressure, which is caused by the lack of interaction force between CO molecules due to the atomic dispersion of Pt on the surface of sample A. The FT-IR spectra confirm that sample A contains only positively charged Pt single atoms, while sample B contains both Pt single atoms and clusters.

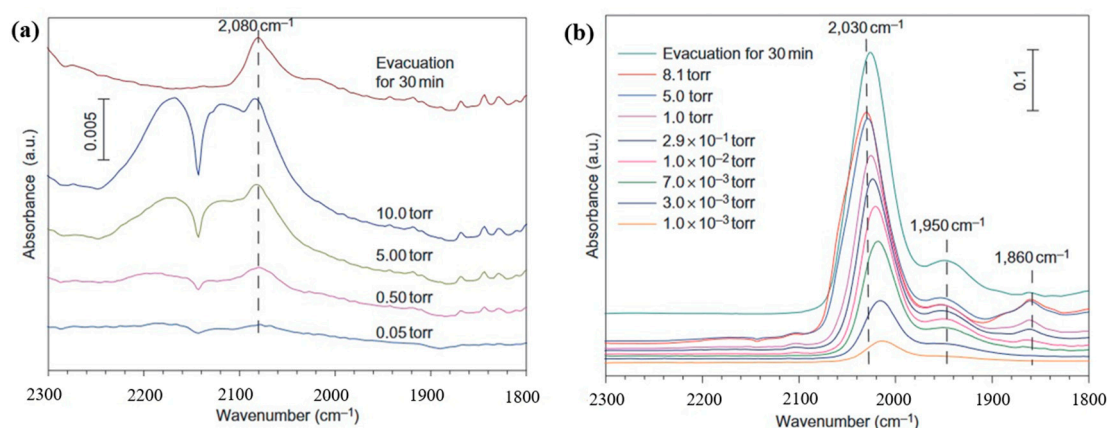


**Figure 6.** (a) In situ FT-IR spectrum of Pt-0.17 wt%-FeO<sub>x</sub> (sample A, FeO<sub>x</sub> with a Pt loading of 0.17 wt%). (b) In situ FT-IR spectrum of Pt-2.5 wt%-FeO<sub>x</sub> (sample B, FeO<sub>x</sub> with a Pt loading of 2.5 wt%). Reprinted with permission from Ref. [71]. Copyright 2011, Springer Nature.

#### 4. Stabilization Strategies of Single Atoms in Metal Oxides

Due to the high surface energy, single atoms tend to migrate and thus agglomerate on the support surface. How to maintain the stability of single atoms on the surface of metal oxides is the primary condition for the preparation of SAC-functionalized metal oxides [72,73]. The interaction between the single atoms and the substrate oxide is what ensures its stability [74]. In 1978, Tauster et al. first introduced the concept of strong metal–support interactions by investigating the reasons for the changes in the adsorption capacity of TiO<sub>2</sub> loaded with noble metal nanoparticles for hydrogen and CO before and after high-temperature reductions and demonstrated that it is such strong metal–support interactions that lead to changes in the adsorption properties of metals [75]. In 2020, Han et al. found that TiO<sub>2</sub> nanosheets loaded with single-atom Pt also showed the complete inhibition of CO adsorption at higher reduction temperatures. This is the interaction between the single-atom Pt and TiO<sub>2</sub> that saturates the Pt atoms with coordination, confirming, for the first time, the existence of strong metal–support interactions in single-atom-loaded

substrate materials [76]. The stronger the interaction between the single atom and the oxide substrate, the less likely the single atom is to migrate, which would thus lead to agglomeration. Therefore, enhancing the interaction between the single atom and the oxide substrate is the key to improving the stability of the single atom. Currently, the commonly used strategies are mainly to enhance the interaction by constructing defects on the support surface, introducing oxygen-containing functional groups and providing spatial confinement through the microporous structure of the support.

#### 4.1. Stabilization through Defects

Reducible metal oxide surfaces are prone to oxygen vacancies [77,78] or metal cation vacancies [79,80], which is an effective strategy for anchoring single atoms. Sanchez and Gazquez proposed a generalized model in which metal atoms interact strongly through lattice vacancies with oxygen ions in metal oxide supports. This strong interaction makes metal atoms nested at surface defects more stable than those on ideal surfaces, which inhibits the sintering of metal atoms under harsh reaction conditions [81]. Wan et al. anchored Pt single atoms at oxygen vacancies on the TiO<sub>2</sub> surface to limit the migration through Ti-Pt strong interactions. The oxygen vacancies were used to stabilize the Au single-atom sites by constructing a Ti-Au-Ti structure while lowering the energy barrier and eliminating the competitive adsorption to improve the catalytic performance. The formation is schematically demonstrated in Figure 7a [82]. In addition, bimetallic active sites can be constructed by utilizing the oxygen vacancies on the surface of metal oxides, Zhang et al. successfully anchored Rh single atoms at the oxygen vacancies on the surface of Co<sub>3</sub>O<sub>4</sub>. In this case, Rh binds to three Co atoms, resulting in the formation of Rh<sub>1</sub>Co<sub>3</sub> bimetallic sites, which is an effective way to develop efficient catalysts [83]. Metal cation vacancies are also common defects on the surface of reducible metal oxides [84]. Qu et al. exploited the formation of triple hollow sites formed by three surface lattice oxygen atoms on the surface of Fe<sub>2</sub>O<sub>3</sub> (001) due to the absence of Fe ions. A single Mo ion occupies such a hollow site. It forms a binuclear site with the neighboring Fe ion (Figure 7b,c), providing a design strategy for developing improved selective catalytic reduction catalysts [85]. As demonstrated by DFT calculations, the Fe cation site is the most stable occupation site for Pt atoms on the 001 surface of Fe<sub>2</sub>O<sub>3</sub>. As shown in Figure 7d–f, the Pt single atoms all occupy the positions of Fe atoms [79].

For irreducible metal oxides, the coordination of unsaturated centers on their surfaces also provides effective sites for anchoring metal atoms. Kwak et al. proposed that the coordination of unsaturated penta-coordination Al<sup>3+</sup> (Al<sup>3+</sup><sub>penta</sub>) on the (100) surface of the  $\gamma$ -Al<sub>2</sub>O<sub>3</sub> surface is the driving force for strong metal–support interactions. At low Pt loading (<1 wt%), the anchoring of Pt atoms through this coordinated unsaturated site forms the atomic dispersion of Pt on the Al<sub>2</sub>O<sub>3</sub> surface [86].

#### 4.2. Stabilization through Surface-O(OH)<sub>x</sub> Species

Anchoring metal single atoms by –O or –OH on the oxide surface is an effective way to load SACs, whether for reducible or non-reducible supports [87–89]. Yang et al. found that the noble metals Au can form –O and –OH bonds with a variety of alkali ions, which in turn lead to the formation of stable single-dot cations Au–O(OH)<sub>x</sub> species. In the catalytic reaction of water–gas shifts, the loaded single-atom Au species have the same catalytic activity for non-reducible carriers such as KLTL zeolite and mesoporous MCM-41 silica and reducible carriers such as cerium dioxide and iron oxide [90]. It was further found that for the three types of supports, TiO<sub>2</sub>, KLTL zeolite, and mesoporous MCM-41 silica, the Pt catalysts without added Na ions existed in large quantities as nanoparticles on all three types of supports. In contrast, more than 80% of the Pt catalysts added with Na ions existed in the form of isolated atoms and did not contain nanoparticles. The addition of Na ions increases the amount of hydroxyl radicals on the surface, which makes it easier for the formation of Pt–O(OH)<sub>x</sub> active species [91]. Wang et al. revealed that the terminal hydroxyl groups on the surface of  $\gamma$ -Al<sub>2</sub>O<sub>3</sub> are essential for anchoring Ag single atoms. The

presence of more abundant terminal hydroxyl groups on the nanoscale  $\gamma$ - $\text{Al}_2\text{O}_3$  compared to the microscale  $\gamma$ - $\text{Al}_2\text{O}_3$  allows the Ag catalyst to form atomic dispersion instead of clusters, leading to higher catalytic performance [89]. The use of  $-\text{O}(\text{OH})_x$  species to achieve anchoring to metal atoms is a more widely applicable method for loading SACs.

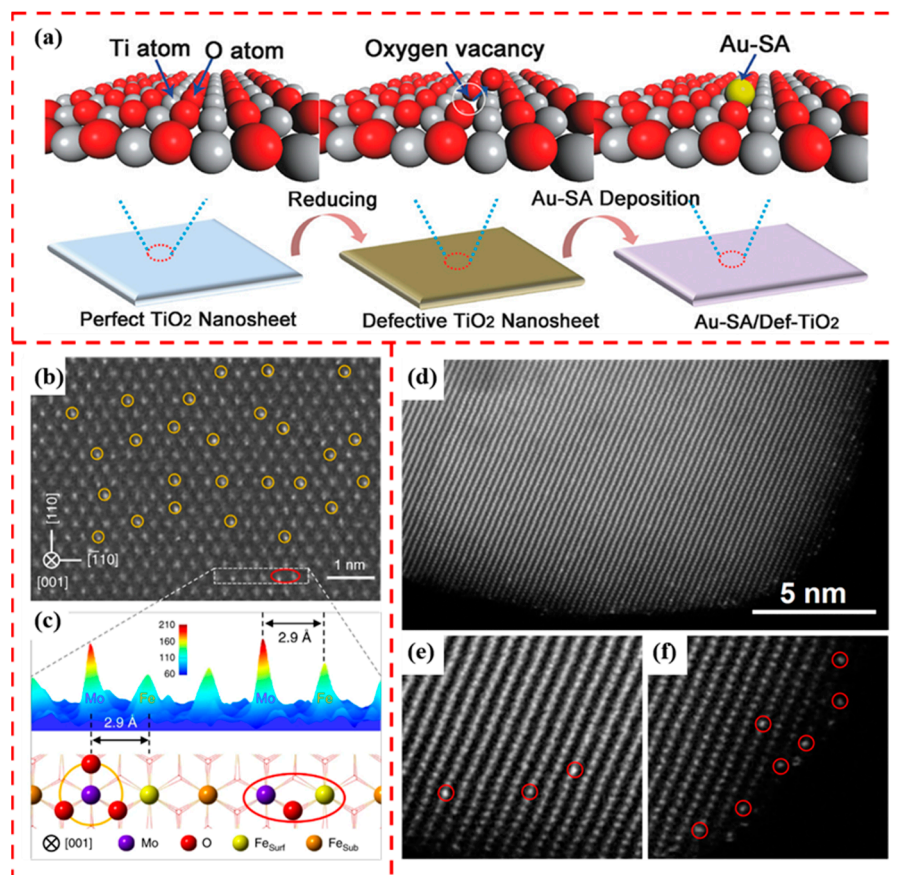


**Figure 7.** (a) Schematic diagram of Au single atoms anchored at oxygen vacancies on the surface of  $\text{TiO}_2$ . Reprinted with permission from Ref. [82]. Copyright 2018, Wiley-VCH Verlag GmbH. (b) AC-STEM image of  $\text{Mo}_1/\text{Fe}_2\text{O}_3$ , where Mo single-atoms are marked with yellow circles. (c) Intensity surface map and structural model of the selected region in (b) (white dashed rectangles). Reprinted with permission from Ref. [85]. Copyright 2020, Springer Nature. (d) Typical high-resolution HAADF-STEM image of  $0.05\text{Pt}_1/\text{Fe}_2\text{O}_3$ . (e) Pt single atoms on the surface of  $\text{Fe}_2\text{O}_3$  are observed as bright spots. (f) Pt single atoms on the surface of  $\text{Fe}_2\text{O}_3$  are occupied by Fe atoms, marked by red circles. Reprinted with permission from Ref. [79]. Copyright 2018, IOP PUBLISHING LTD.

#### 4.3. Stabilization through Spatial Constraints

The rational design of the internal pores of a material is also a strategy to stabilize single-atom catalysts. The spatial confinement of individual atoms by using pores can inhibit SAC sintering [92–94]. Carbon-based materials and zeolite series materials are characterized by their porous nature and are widely used as supports for anchoring SACs [95–97]. In addition, there have also been some studies on synthesizing metal oxides with porous structures as supports for anchoring SACs [98]. Ye et al. synthesized  $12\text{CaO} \cdot 7\text{Al}_2\text{O}_3$  material (C12A7) with a unique cage-like structure. The cavity of this cage-like structure is positively charged and interacts with the metal anion to achieve metal anion separation. The cavity size of 0.4 nm is just suitable for accommodating single metal atoms (Figure 8a). The unique stabilizing effect of the cavity nanostructures on the Pt single atoms was demonstrated by theoretical simulations and experimental characterization, and they remained atomically dispersed at a high temperature of 600 °C [99]. Zhang et al. loaded

Pt catalysts on the surface of  $\text{Al}_2\text{O}_3$  materials with and without mesoporous structure and confirmed that the mesoporous structure and the unique inner surface skeleton play a decisive role in achieving the atomic dispersion of Pt by comparing the results of the material characterization [93].

The use of heterojunctions to achieve the spatial confinement of the SAC is also an effective method. Shin et al. used metal oxide nano-heterostructures to achieve the effective stabilization of Pt SACs (Figure 8b). The heterojunction composed of carbon nitride/ $\text{SnO}_2$  not only spatially confines the Pt single-atom catalyst but also participates in the catalysis of the surface reaction of formaldehyde gas detection, which greatly improves the catalytic performance of the SACs system [100]. Enhancing the interaction between SACs and metal oxide support through the spatial restriction of porous structures or heterojunctions can inhibit the sintering failure of SACs. However, there are still few studies on this aspect, and it is necessary to explore more kinds of metal oxide supports further to achieve the anchoring of SACs through spatial confinement.

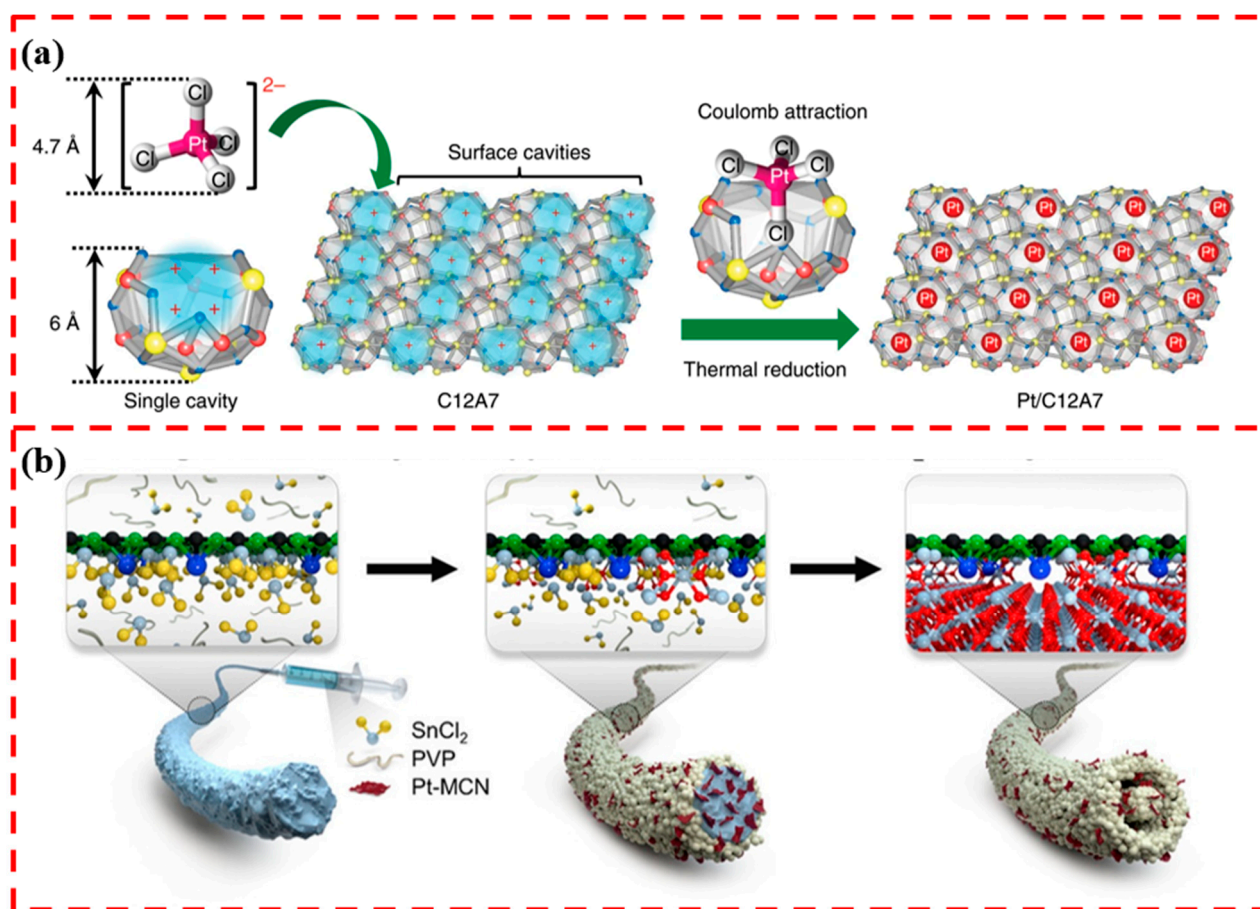


**Figure 8.** (a) Schematic representation of the positively charged surface cavity of C12A7 stabilizing a single Pt atom. Reprinted with permission from Ref. [99]. Copyright 2020, Springer Nature. (b) Pt single-atom catalyst stabilized at the carbon nitride/ $\text{SnO}_2$  heterojunction. Reprinted with permission from Ref. [100]. Copyright 2020, American Chemical Society.

### 5. Gas-Sensitive Properties of SAC-Functionalized Metal Oxides

At present, applications regarding metal oxide gas-sensitive materials functionalized with SACs are mainly focused on  $\text{SnO}_2$ ,  $\text{WO}_3$ ,  $\text{ZnO}$ , and  $\text{In}_2\text{O}_3$ . In addition,  $\text{Fe}_2\text{O}_3$ ,  $\text{TiO}_2$ , and  $\text{Co}_3\text{O}_4$  functionalized by SACs have also been reported, but with fewer studies. The existing studies are discussed in detail in this section.

### 5.1. SnO<sub>2</sub>-Based Support

SnO<sub>2</sub> is the first commercialized gas sensor, and it is one of the most studied metal oxide materials for its excellent gas-sensitive response, high stability, and low cost [101,102]. The surface modification of SnO<sub>2</sub> by single atoms has developed a new potential for SnO<sub>2</sub> as a gas-sensitive material [103–106]. In 2020, Xu et al. developed Pt single-atom-modified SnO<sub>2</sub> thin-film sensitive materials, which is the first report of Pt single-atom-catalyst-modified SnO<sub>2</sub> for gas-sensing applications [107]. The ALD technique was used to deposit SnO<sub>2</sub> films on SnO<sub>2</sub>/Si wafers and Pt SACs on SnO<sub>2</sub> films with trimethyl(methylcyclopentadienyl)platinum (IV) (MeCpPtMe<sub>3</sub>) (99%) and O<sub>3</sub> as the precursors. Compared with the pristine SnO<sub>2</sub>, the Pt/SnO<sub>2</sub>-based sensor has a 60 °C lower optimal operating temperature (Figure 9a) and a response up to 136.2 for 10 ppm TEA, which is seven times higher than that of the pristine SnO<sub>2</sub> (20.3). Meanwhile, Pt/SnO<sub>2</sub> has a faster response/recovery time, reaching an ultra-high sensitivity of 8.76 ppm<sup>-1</sup> and a very low limit of detection (LOD) of 7 ppb (Figure 9b–d). By SEM characterization, the structure of Pt/SnO<sub>2</sub> was unchanged compared with the SnO<sub>2</sub> film (Figure 9e,f). Brighter contrast images of Pt single atoms uniformly dispersed on SnO<sub>2</sub> were obtained using high-angle annular dark-field scanning transmission electron microscopy (HAADF-STEM) (Figure 9g,h), confirming the successful loading of Pt single atoms. The single platinum atoms loaded on SnO<sub>2</sub> have a chemical sensitization effect that dissociates atmospheric oxygen molecules into negatively charged oxygen ions, thereby increasing the adsorbed oxygen on the surface of tin dioxide. This feature improves the gas-sensitive properties of Pt/SnO<sub>2</sub>. In the meantime, the presence of single Pt atoms can reduce the activation energy of the surface reaction and enhance the adsorption and desorption of TEA. Zhou et al. prepared single-atom Rh-modified SnO<sub>2</sub> nanoparticle-sensitive materials for formaldehyde detection by ALD [102]. The response of Rh/SnO<sub>2</sub> to 20 ppm formaldehyde was 36.3, which was about 23 times higher than that of pure SnO<sub>2</sub>, and the response and recovery times were 4 s and 9 s, respectively. DFT theoretical calculations revealed that the reason for the improved gas-sensitive performance was that the Rh atoms increased the adsorption and charge transfer between formaldehyde molecules and SnO<sub>2</sub>.

In addition to noble metal SACs modification, non-precious metal single-atom modification on the surface of SnO<sub>2</sub> also has excellent gas-sensitive response properties. Liu et al. loaded a Ni single atom on the surface of SnO<sub>2</sub> by impregnation. K-edge X-ray absorption near-edge structure (XANES) results showed that the valence of Ni in SAC-Ni/SnO<sub>2</sub> was at +2, and there were no observed Ni-Ni coordination-related FT-EXAFS peaks, which suggests that only single Ni atoms are present in SnO<sub>2</sub>, and no Ni nanoparticles are present [108]. The O<sub>3</sub>C vacancy and cavity SAC-Ni are candidate sites for capturing SO<sub>2</sub>. SAC-Ni adsorbs SO<sub>2</sub> and then reacts with superoxide radicals generated from nearby oxygen vacancies to achieve the highly selective detection of SO<sub>2</sub> (Figure 9i), demonstrating that the designed SAC-Ni/H-SnO<sub>2</sub> sensor is reasonable and effective. The SAC-Ni/H-SnO<sub>2</sub> sensor with Ni single-atom loading and enriched with oxygen vacancies showed a response value of 48 for 20 ppm SO<sub>2</sub> and a detection limit of 100 ppb. DFT theoretical calculations showed that the oxygen vacancies and SAC-Ni are the candidate sites for the capture of SO<sub>2</sub>. Therefore, the gas-sensitive performance of SAC-Ni/H-SnO<sub>2</sub> was substantially improved compared to SnO<sub>2</sub>.

Inorganic supports have the disadvantages of having a small area and a lack of stable defect sites compared to organic or organic–inorganic composite supports, resulting in relatively low single-atom catalyst loadings (<1 wt%). Shin et al. developed a general method for the preparation of SACs on metal and metal oxide supports by using N-doped graphene as a spatially confined single-atom sacrificial template [109]. Inductively coupled plasma atomic emission spectroscopy results showed successful loading up to 2.12 wt% of Pt single atoms on SnO<sub>2</sub> nanosheets. The Pt-SA-functionalized Pt<sub>1</sub>-SnO<sub>2</sub> NSs sensors exhibited superior sensitivity for acetone detection. For 10 ppm acetone, the response values of Pt<sub>1</sub>-SnO<sub>2</sub> NSs were improved by 7.6-fold and 4.0-fold, respectively, compared to the original SnO<sub>2</sub> NSs (R<sub>air</sub>/R<sub>gas</sub> = 12.6) and Pt<sub>n</sub>-SnO<sub>2</sub> (R<sub>air</sub>/R<sub>gas</sub> = 23.8).

SAC-functionalized SnO<sub>2</sub> sensitive materials show surprising gas-sensitive properties. The selection of suitable single atoms for synergistic interactions with SnO<sub>2</sub> provides a new strategy for the enhancement of gas-sensitive performance.

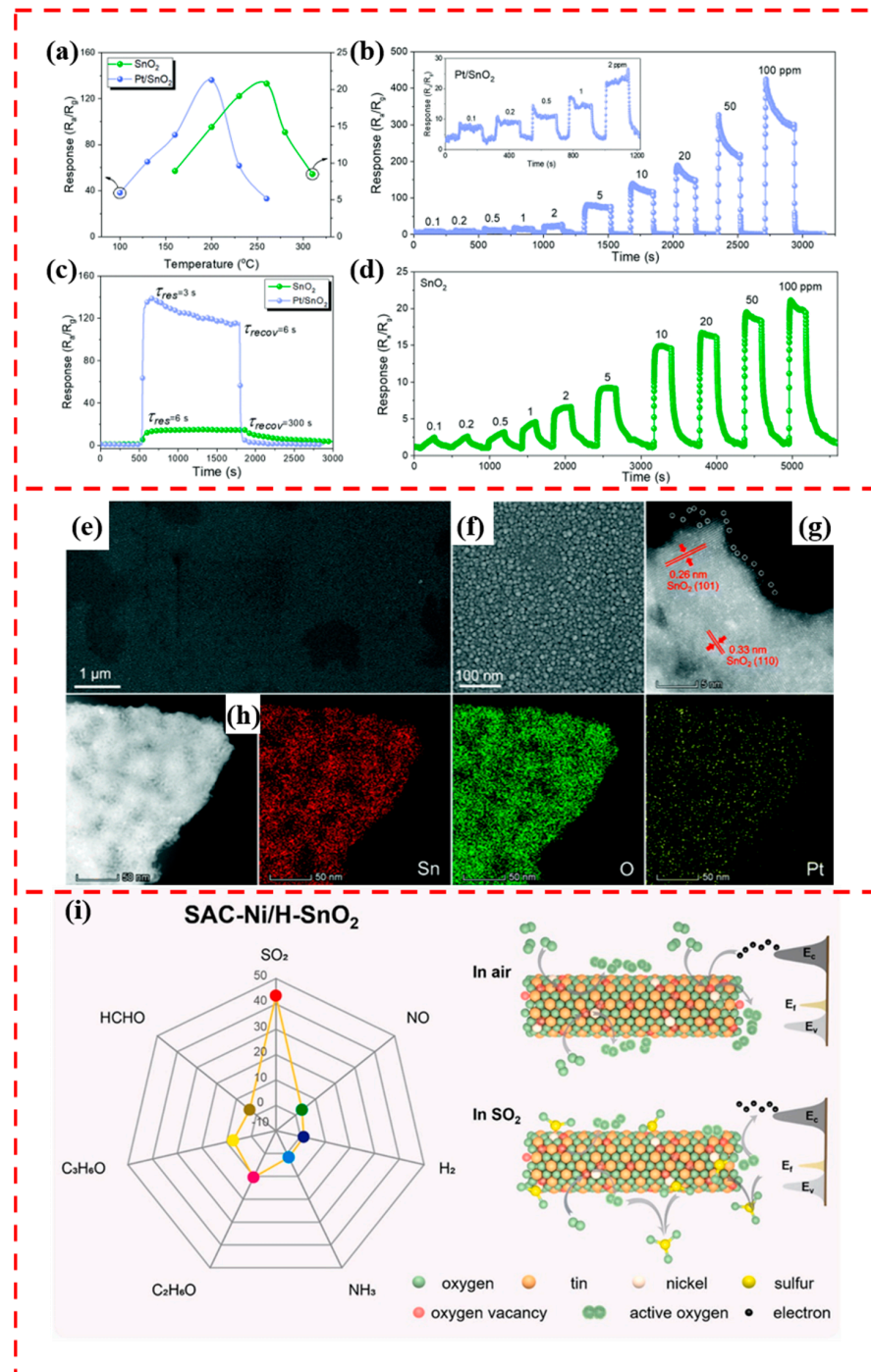


**Figure 9.** (a) Response of SnO<sub>2</sub> and Pt/SnO<sub>2</sub> films to 10 ppm TEA at different temperatures. (b) Response of Pt/SnO<sub>2</sub> films to 0.1–100 ppm TEA at 200 °C. (c) Dynamic response of SnO<sub>2</sub> and Pt/SnO<sub>2</sub> films to 10 ppm TEA at 200 °C. (d) Response of SnO<sub>2</sub> films to 0.1–100 ppm TEA at 200 °C. (e,f) SEM image of SnO<sub>2</sub> film. (g) HAADF-STEM image. (h) EDS STEM elemental mapping of single-atom Pt/SnO<sub>2</sub> film. Reprinted with permission from Ref. [107]. Copyright 2020, ROYAL SOC CHEMISTRY. (i) Schematic representation of the selectivity of SAC-Ni/H-SnO<sub>2</sub> to different gases at 250 °C, 40% RH, and sensing of SO<sub>2</sub>. Reprinted with permission from Ref. [108]. Copyright 2022, Elsevier.

## 5.2. $WO_x$ -Based Support

$WO_3$  is an n-type semiconductor with a low bandgap (2.8 eV), which has the advantages of a superior charge transfer capability, good stability, and easy preparation. Therefore,  $WO_3$  has gradually become a popular gas-sensitive material. However, the performance of pure  $WO_3$  cannot fully meet the needs of practical applications, and the modification of its surface by adding noble metals is a way to improve the gas sensing performance [110]. Gu et al. prepared three kinds of sensitive materials, pure  $WO_3$ , single-atom Pt-loaded  $WO_3$ , and Pt nanocluster-loaded  $WO_3$ , and designed gas sensors, denoted as  $WO_3$ , SA-Pt/ $WO_3$ , and NC-Pt/ $WO_3$ , for the detection of triethylamine and trimethylamine gases produced by fish spoilage [111]. The optimal operating temperature of the SA-Pt/ $WO_3$  gas sensors was reduced by 20 °C compared to  $WO_3$ . Although the Pt loading in NC-Pt/ $WO_3$  is higher than that in SA-Pt/ $WO_3$ , SA-Pt/ $WO_3$  has the best TEA detection among the three, with a sensitivity of 28.37 ppm<sup>-1</sup> and a detection limit of 0.18 ppb. This is because of the atomic dispersion results in the exposure of every Pt atom and the formation of reactive sites, which leads to a higher adsorbed oxygen content in SA-Pt/ $WO_3$  than in NC-Pt/ $WO_3$ . The superior TEA detection properties of SA-Pt/ $WO_3$  were attributed to the high adsorbed oxygen content and low activation energy. Yuan et al. loaded Pt single atoms and Pt nanoparticles on the surface of  $WO_{3-x}$ , which is rich in oxygen vacancies. The surface atoms of the nanoparticle Pt have many coordination environments compared to single Pt atoms, while the individual atoms exist in similar chemical states. The SA-Pt/ $WO_{3-x}$  gas sensor not only has a higher response compared to Pt nanoparticle-loaded  $WO_{3-x}$  (Figure 10a,b) but also exhibits a high selectivity for acetone (Figure 10c) [112].

The synergistic interaction of rationally designed noble metal single atoms with oxygen vacancies or transition metal atoms on the surface of  $WO_3$  has significant advantages for enhancing gas-sensitive properties. It has been shown that Ag single atoms deposited on the surface of  $WO_3$  promote the formation of incomplete valence  $W^{5+}$ , which increases the oxygen vacancy content [113]. The Ag single atoms on the surface of  $WO_3$  act as active sites, lowering the energy barrier and improving the adsorption performance of the target gas. Oxygen vacancies as active sites increased the rate of oxygen adsorption (Figure 10d). Therefore, at the most suitable Ag loading, the Ag- $WO_3$ -2 (pure  $WO_3$  under 0.01 mol L<sup>-1</sup> silver nitrate solution), detected via a low-temperature deposition sensor, exhibited a superior gas-sensitive performance with a 5150 response for 50 ppm TEA target gas at 175 °C, a detection limit of 1.7 ppb, and long-term stability as well as high selectivity and reproducibility. Gu et al. synthesized Pt-loaded three-dimensionally ordered microporous (3DOM)  $WO_3$ -sensing materials. The addition of Co and Ni led to the formation of more oxygen vacancies on the surface of the  $WO_3$ -sensing material, which resulted in the richer surface adsorption of oxygen [114]. Adding Co and Ni leads to more oxygen vacancies on the  $WO_3$  surface, resulting in the richer surface adsorption of oxygen. Meanwhile, the addition of Co and Ni narrows the band gap of the sensitive materials. It promotes the increase in electron mobility, which contributes to improving the sensing performance. 3DOM PtCo- $WO_3$  and PtNi- $WO_3$  exhibit high selectivity and sensitivity for xylene detection. Among them, the 3DOM PtCo- $WO_3$  with atomically dispersed Pt exhibited the most heightened sensitivity of 3.91 ppm<sup>-1</sup> and the lowest detection limit of 1.08 ppb, and its sensing process is shown in Figure 10e. Researchers can explore more kinds of single atoms interacting with  $WO_3$  support to enhance gas-sensitive performance.

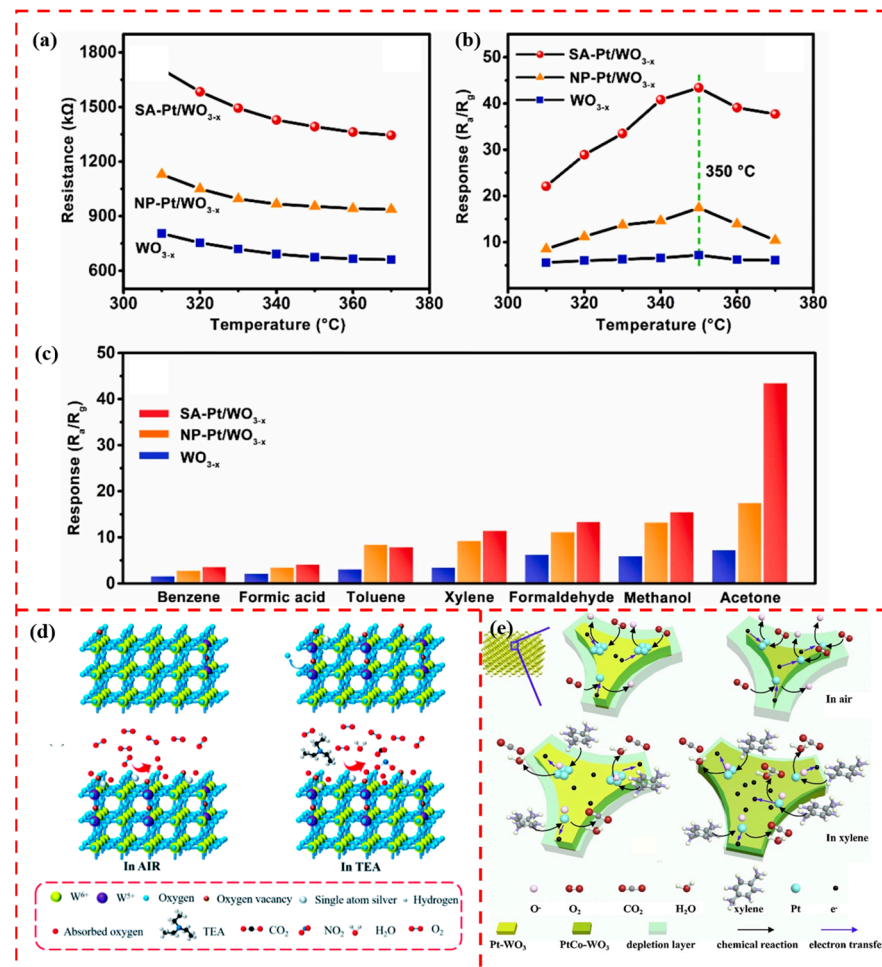


**Figure 10.** (a) Resistance change in air at different temperatures. (b) Response to 5 ppm acetone at different operating temperatures, which all reach optimal response at 350°C and (c) selectivity test for WO<sub>3-x</sub>, NP-Pt/WO<sub>3-x</sub>, and SA-Pt/WO<sub>3-x</sub> for different vapors at 5 ppm (T = 350 °C, RH = 40%). Reprinted with permission from Ref. [112]. Copyright 2023, Elsevier. (d) Schematic representation of WO<sub>3</sub> before and after loading with single-atom Ag and schematic representation of the reaction mechanism of single-atom Ag-loaded WO<sub>3</sub> in air and TEA. Reprinted with permission from Ref. [113]. Copyright 2021, ROYAL SOC CHEMISTRY. (e) Sensing mechanism diagrams of Pt-WO<sub>3</sub> and PtCo-WO<sub>3</sub> samples. Reprinted with permission from Ref. [114]. Copyright 2019, Elsevier.

### 5.3. ZnO-Based Support

ZnO, another common n-type metal oxide semiconductor, is also one of the most studied sensitive materials for gas sensors [115]. ZnO has abundant nanostructures, and different nanostructures can provide various anchoring sites for the loading of SACs. For example, Xue et al. developed a freestanding ladder-like ZnO surface with many unsaturated step defects by controlling the temperature and solvent environment of the reaction system (Figure 11a) [116]. DFT theoretical calculations confirmed that the anchoring of Au single atoms was more stable at the step positions than at the surface positions. The gas-sensitive properties of Au<sub>1</sub>-ZnO, Au-NP-ZnO, and ZnO were further investigated, and the Au<sub>1</sub>/ZnO gas sensors achieved a 12.6-fold response to 300 ppb NO<sub>2</sub> at 150 °C, which is 1.6-fold and 7-fold higher than that of the Au-NP-ZnO and ZnO sensors, respectively. The Au single atom promotes the activation reaction between NO<sub>2</sub> and the adsorbed oxygen by facilitating the interaction between NO<sub>2</sub> and the electron transfer between the support. Liu et al. anchored Pt single atoms on ZnO nanorods (Figure 11b) to achieve the ultra-sensitive detection of triethylamine gas [117]. Pt-NP/ZnO and Pt<sub>1</sub>/ZnO were characterized and analyzed by XPS and EXAFS, and the binding energy of Pt<sup>2+</sup> in Pt<sub>1</sub>/ZnO showed a sig-

nificant blue shift compared to that of Pt-NP/ZnO, suggesting the presence of a charge transfer between single Pt atoms and the surface of ZnO. The Pt<sub>1</sub>/ZnO samples had only Pt-O coordination peaks, indicating that the Pt atoms existed in an isolated state. The Pt-NP/ZnO has a characteristic peak of Pt-Pt coordination, reflecting the presence of Pt in the form of clustered nanoparticles (Figure 11c). DRIFTS analysis, using CO as a probe molecule, showed the presence of only 2092 cm<sup>-1</sup> single bands in the Pt<sub>1</sub>/ZnO sample, demonstrating the presence of Pt<sup>n+</sup> in the absence of metallic Pt (Figure 11c). The Pt<sub>1</sub>/ZnO gas sensor achieved a 4170-fold response to 100 ppm TEA at 200 °C, which is 92 times that of pure ZnO. Also, the response time (34 s) and recovery time (76 s) were shorter (Figure 11d). DFT calculations showed that the effective adsorption and activation of the TEA molecules on the Pt<sub>1</sub>/ZnO facilitated the interaction between the TEA molecules and the reactive oxygen species, which significantly improved the sensing performance of the Pt<sub>1</sub>/ZnO sensor.

Rong et al. synthesized a porous Ag-LaFeO<sub>3</sub>@ZnO core-shell sphere structure by isolating the Pt monoatomic precursor with the help of the porous structure of ZIF-8 and removing the ligand from the precursor by subsequent heat treatment [118]. The dispersion of Pt<sub>1-2</sub> atoms on the porous Ag-LaFeO<sub>3</sub>@ZnO support significantly enhanced the adsorption energy of methanol and oxygen on the surface of the sensitive material and promoted the diffusion, adsorption, and reaction of methanol and oxygen on the surface of Ag-LaFeO<sub>3</sub>@ZnO. The Ag-LaFeO<sub>3</sub>@ZnO-Pt sensor has a response of 453.80 for 5 ppm methanol gas at a lower operating temperature of 86 °C. The study of SAC-functionalized ZnO reveals that the morphology of the material has a great influence on the loading of SAC. This feature can also be applied to other metal oxide materials.

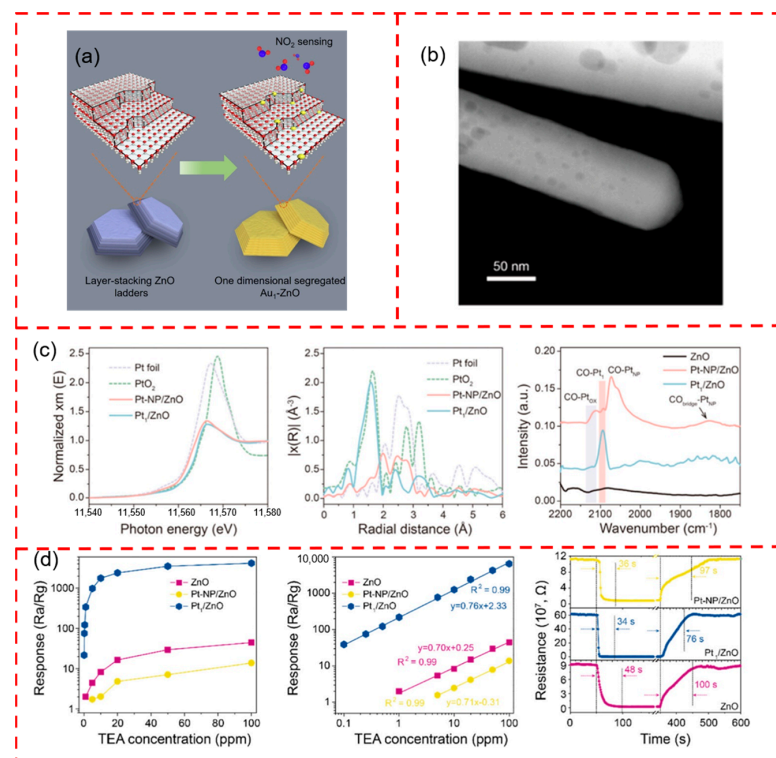


**Figure 11.** (a) Schematic representation of Au single atom anchored at the unsaturated step position of ZnO. Reprinted with permission from Ref. [116]. Copyright 2020, Elsevier. (b) TEM image of Pt<sub>1</sub>/ZnO. (c) XANES spectrograms of ZnO, Pt-NP/ZnO, Pt<sub>1</sub>/ZnO, EXAFS spectra of Pt K-edge, and CO-DRIFTS spectra. (d) The plot of response variation in individual sensors of ZnO, Pt-NP/ZnO, and Pt<sub>1</sub>/ZnO in the range of TEA concentration from 0.1 to 100 ppm, linear relationship plot, and recovery of response in 100 ppm TEA. Reprinted with permission from Ref. [117]. Copyright 2023, American Chemical Society.

#### 5.4. $\text{In}_2\text{O}_3$ -Based Support

Several scholars have investigated the gas-sensitive properties of  $\text{In}_2\text{O}_3$  modified with single atoms of noble metals Au, Pt, and Pd. Gu et al. loaded atomically dispersed Au on  $\text{In}_2\text{O}_3$  nanosheets by the ultraviolet (UV)-assisted reduction method [119]. In situ, CO-DRIFTS, XPS, and other characterization techniques confirmed the successful loading of Au single atoms. In a series of samples with different Au loadings, 0.25% Au/ $\text{In}_2\text{O}_3$  achieved a maximum response value of 85.67 in formaldehyde gas at 100 °C at 50 ppm. The atomically dispersed Au reduces the activation energy required for the reaction and increases the number of reactive sites. The homogeneity of the single-atom active sites resulted in a higher selectivity of the sensitive material for the adsorption of formaldehyde (Figure 12a). Li et al. successfully loaded Au single atoms on the surface of  $\text{In}_2\text{O}_3$  porous nanospheres for the rapid detection of CO [120]. The XPS results show that single-atom Au interacts with the support and therefore exists in an ionic state. In the detection of reducing gases such as CO,  $\text{CH}_4$ ,  $\text{H}_2\text{S}$ , and  $\text{C}_7\text{H}_8$ , pure  $\text{In}_2\text{O}_3$  showed poor selectivity for CO. The Au single-atom-loaded  $\text{Au}_1/\text{In}_2\text{O}_3$ -2 sensor exhibited significantly enhanced selectivity for CO (Figure 12b). The selectivity to CO demonstrates the potential of  $\text{Au}_1/\text{In}_2\text{O}_3$ -2 for application in coal mining environments.

The valence state of single atoms loaded on the surface of  $\text{In}_2\text{O}_3$  also affects the gas-sensitive properties of the material to a great extent. Gu et al. investigated the sensing properties of Pt-loaded  $\text{In}_2\text{O}_3$  nanosheets for triethylamine before and after hydrogen treatment [121]. HAADF-STEM, EXAFS, and XANES characterizations confirmed that the Pt on the surface of 0.25 Pt/ $\text{In}_2\text{O}_3$  samples was highly dispersed before and after hydrogen treatment. In the gas-sensitive performance test of TEA, the hydrogen-treated 0.25 Pt/ $\text{In}_2\text{O}_3$  ( $\text{H}_2$ ) sensor had a lower operating temperature and higher response value than the non-hydrogen-treated 0.25 Pt/ $\text{In}_2\text{O}_3$  sensor at the same test concentration. The analysis of the XPS results showed a higher adsorbed oxygen content on the surface of the  $\text{In}_2\text{O}_3$  after hydrogen treatment. The lower valence state of surface-loaded Pt is more favorable for adsorbed oxygen generation. Pt loading and hydrogen treatment can improve the electron mobility of  $\text{In}_2\text{O}_3$ . The increase in the amount of low-valence Pt after hydrogen treatment promotes the adsorbed oxygen generation. It lowers the TEA response energy barrier, thus increasing the sensitivity of the material to TEA.

Liu et al. took advantage of the porous and surface functional group-rich nature of In-MOFs as a scaffold to support Pd precursor ions [56]. This metal–organic framework template method was employed to synthesize Pd single-atom-loaded  $\text{In}_2\text{O}_3$  with the increase in Pd loading, and Pd single atoms aggregated into PdO nanoparticles. In detecting  $\text{H}_2\text{S}$  gas, the Pd single-atom-loaded  $\text{In}_2\text{O}_3$  showed the highest response to  $\text{H}_2\text{S}$  with high selectivity compared to Pd nanoparticles and PdO nanoparticle-loaded  $\text{In}_2\text{O}_3$  sensors. The Pd single atom has an oxidation state different from other forms of Pd and exists as a positive valence state on the surface of  $\text{In}_2\text{O}_3$ . This special valence state makes the Pd single atom more active. The Pd single-atom catalysts were able to significantly reduce the potential barrier of the  $\text{H}_2\text{S}$  gas decomposition reaction, which increased the number of electrons transferred from the  $\text{H}_2\text{S}$  molecule to the active site of the Pd atom, the sensing process of which is shown in Figure 12c. This indicates that the Pd single-atom catalyst can effectively change the kinetic process of the gas-sensitive reaction. More kinds of single-atom interactions with  $\text{In}_2\text{O}_3$  are expected to be further explored by researchers.

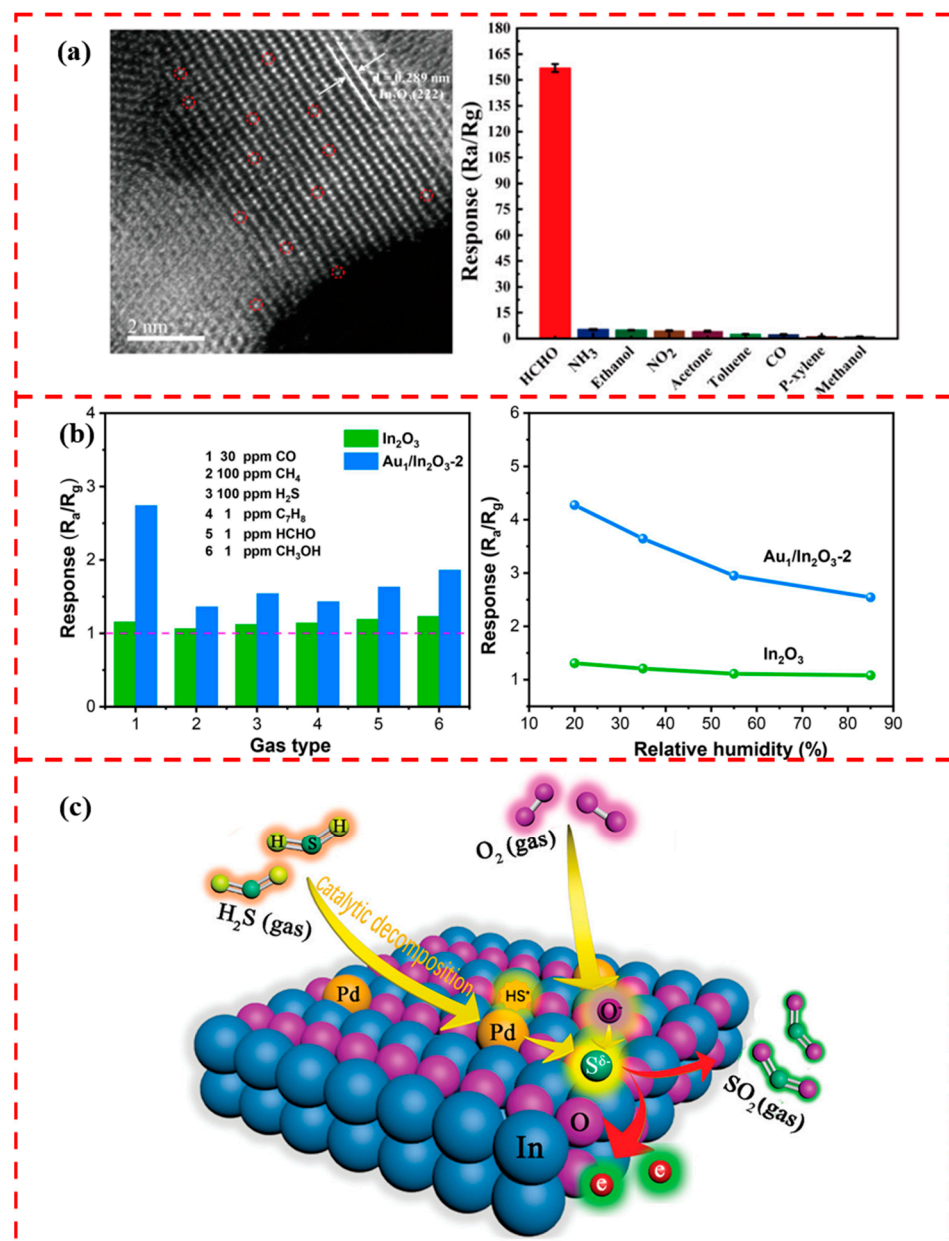


**Figure 12.** (a) HAADF-STEM image of single-atom Au-modified  $\text{In}_2\text{O}_3$ , where red circles highlight monodisperse Au atoms and its high selectivity to formaldehyde gas. Reprinted with permission from Ref. [119]. Copyright 2020, American Chemical Society. (b) High selectivity and humidity resistance of  $\text{Au}_1/\text{In}_2\text{O}_3$  to CO. Reprinted with permission from Ref. [120]. Copyright 2023, Elsevier. (c) Schematic diagram of Pd single-atom-loaded  $\text{In}_2\text{O}_3$  sensing to  $\text{H}_2\text{S}$  gas. Reprinted with permission from Ref. [56]. Copyright 2021, John Wiley and Sons.

### 5.5. Other Metal Oxides-Based Supports

In the study of metal oxide gas-sensitive materials modified by single-atom catalysts, the  $\text{SnO}_2$ ,  $\text{WO}_3$ ,  $\text{ZnO}$ , and  $\text{In}_2\text{O}_3$  mentioned above are the more studied supports. Some other metal oxide-related reports appeared. For example, Li et al. loaded single-atom Pt on porous  $\gamma\text{-Fe}_2\text{O}_3$  nanoparticles, achieving an efficient detection of ethanol [122]. The  $\text{Pt}_1\text{-Fe}_2\text{O}_3\text{-ox}$  sensor with a higher oxidation state Pt exhibited a higher response to ethanol gas (Figure 13a) because the high-valent Pt single atom can effectively increase the adsorption capacity of ethanol gas through charge transfer with an  $\text{Fe}_2\text{O}_3$  support, which improves the gas sensing performance. Ye et al. synthesized Pd single-atom-modified  $\text{TiO}_2$  nanoflowers by the photochemical method for CO gas sensing [123]. In situ DRIFT

characterizations showed that Pd<sub>1</sub>-TiO<sub>2</sub> had the strongest adsorption capacity for CO at the same exposure time, higher than Pd-NPs-TiO<sub>2</sub> and TiO<sub>2</sub>. Five individually fabricated Pd<sub>1</sub>-TiO<sub>2</sub> gas sensors achieved an average response of (12,549 ± 494)% to 100 ppm CO at room temperature, the highest value of all the reported sensitive materials operating at room temperature (Figure 13b). Meanwhile, the Pd<sub>1</sub>-TiO<sub>2</sub> showed excellent CO selectivity in 12 common interfering gases. Koga explored the effect of Pd loading on the hydrogen-sensing performance of mesoporous p-type Co<sub>3</sub>O<sub>4</sub> nanoparticles [124]. The loading of Pd single atoms on the surface of Co<sub>3</sub>O<sub>4</sub> could reach up to 5%, and a further increase in loading led to the formation of Pd oxide clusters. Pd single atoms existed at +4 valence on the surface of Co<sub>3</sub>O<sub>4</sub>, and after exposure to 1000 ppm H<sub>2</sub>, about 10% of Pd<sup>4+</sup> was reduced to Pd<sup>2+</sup>. It is suggested that the catalytic redox process from Pd<sup>4+</sup> to Pd<sup>2+</sup> accelerated hydrogen sensing, which enhanced the sensitivity and speed of Co<sub>3</sub>O<sub>4</sub> response to hydrogen gas (Figure 13c). At present, the studies of metal oxide gas-sensitive materials modified by SACs are still scarce, and more kinds of metal oxides combined with SACs with gas-sensitive properties need to be discovered by further research.

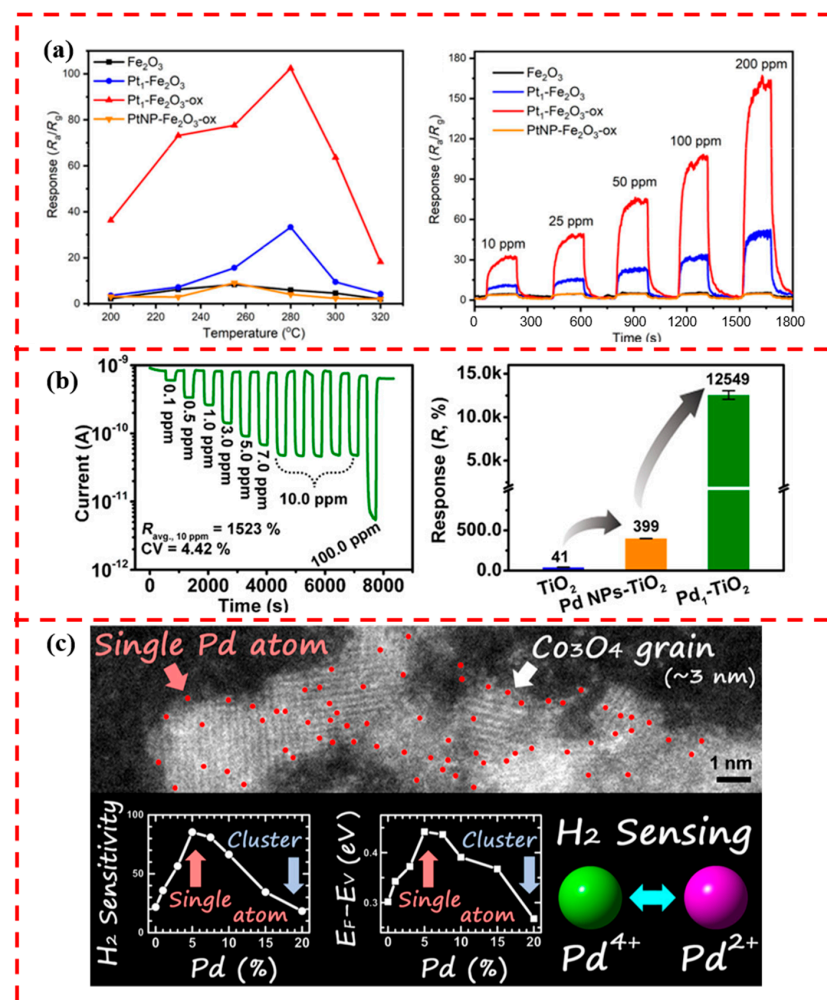


**Figure 13.** (a) Response of Fe<sub>2</sub>O<sub>3</sub>, Pt<sub>1</sub>-Fe<sub>2</sub>O<sub>3</sub>, and Pt<sub>1</sub>-Fe<sub>2</sub>O<sub>3</sub>-ox to 100 ppm C<sub>2</sub>H<sub>5</sub>OH at operating temperature of 200–320 °C to 10–200 ppm concentration of C<sub>2</sub>H<sub>5</sub>OH at 280 °C. Reprinted with permission from Ref. [122]. Copyright 2021, Springer Nature. (b) Response curves of Pd<sub>1</sub>-TiO<sub>2</sub> to CO in the concentration range of 0.1–100 ppm at room temperature and histograms of pristine TiO<sub>2</sub>, Pd-NPs-TiO<sub>2</sub>, and Pd<sub>1</sub>-TiO<sub>2</sub> nanoflowers to 100 ppm CO. Reprinted with permission from Ref. [123]. Copyright 2021, American Chemical Society. (c) Plot of Pd in the form of loading on the surface of Co<sub>3</sub>O<sub>4</sub> as a function of loading amount. Reprinted with permission from Ref. [124]. Copyright 2020, American Chemical Society.

## 6. Summary and Perspectives

In this review, we summarize the progress and utilization of SACs in the metal oxide-based gas sensors, involving the synthesis and characterization methods, stabilization strategies, and gas sensing performance of SACs. The sensing performance of SACs and other modification strategies are summarized in Table 1. As for the heterostructured and MOF-derived metal oxide strategies, they may help detect gases at room temperature, while SACs need a relatively high temperature. In comparison with the modification of normal micro-nanostructures, and nanoparticles decoration strategies, the SAC decoration strategy shows some advantages regarding response, response/recovery time, and selectivity. In conclusion, SACs have made achievements in some aspects of gas sensing, such as response, response/recovery time, and selectivity. However, the application of SACs in the field of gas sensitivity is still in the initial stage. There are still some important issues that need to be further explored and researched:

**Table 1.** The sensing performance summary of SAC and other strategies.

Material	Strategy	Response	Conc. [ppm]	Temp. [°C]	Response/Recovery Time [s]	Analytes	Ref.
3D Networks ZnO	Micro-Nanostructures	3.338	1600	25	20/>60	ethanol	[125]
WO <sub>3</sub> /ZnO	Heterostructured	96	100	200	45/1350	Triethylamine	[126]
MOF-NiO/SnO <sub>2</sub>	MOF-Derived	5.48	100	25	56/4	CO	[127]
In <sub>2</sub> O <sub>3</sub> /SnO <sub>2</sub>	Heterostructured	1.8	10	240	80/60	SO <sub>2</sub>	[19]
CuO/In <sub>2</sub> O <sub>3</sub>	Nanoparticles Decoration	231.2	100	140	9/17	HCHO	[128]
Pt NCs@SnO <sub>2</sub> @SiC	Noble Metal Decoration	56	500	300	/	ethanol	[103]
Dy doping In <sub>2</sub> O <sub>3</sub>	Doping	85	100	250	5/248	ethanol	[129]
Ag NCs In <sub>2</sub> O <sub>3</sub>	Noble Metal decoration	35.6	100	270	25/43	ethanol	[130]
Zn doping In <sub>2</sub> S <sub>3</sub> /In <sub>2</sub> O <sub>3</sub>	Doping	45	100	100	11/24	ethanol	[131]
Pt SAs@SnO <sub>2</sub> @SiC	Single-Atom Catalysts	119	500	350	15/20	ethanol	[103]
Pt-In <sub>2</sub> O <sub>3</sub>	Single-Atom Catalysts	750	100	200	2/373	HCHO	[132]
Pt SA-SnO <sub>2</sub>	Single-Atom Catalysts	25	5	175	/	HCHO	[133]
Ni SA/SnO <sub>2</sub>	Single-Atom Catalysts	50	40	250	52/45	SO <sub>2</sub>	[108]
Ag SA-WO <sub>3</sub>	Single-Atom Catalysts	4700	50	175	189/1354	Triethylamine	[113]
Pt SA-ZnO	Single-Atom Catalysts	4170	100	175	34/76	Triethylamine	[117]

(1) The high surface energy of the single atom tends to migrate and agglomerate on the support surface, resulting in catalyst deactivation. At the same time, single atoms tend to anchor at the defects and functional groups on the support surface, and the number of surface defects or functional groups limits the loading content. Due to the above reasons, SACs on the support surface are prone to agglomerate and deactivate under harsh environments such as high temperatures, and the loading content of single atoms generally does not exceed 1 wt%. Therefore, achieving the high stability and high-loading anchoring of SACs is important. The development of an efficient, stable, and versatile synthesis method for SACs is the key to promoting the application of SACs in gas-sensitive fields, which is the problem.

(2) At present, research on the application of SACs in metal oxide-based gas-sensitive materials mainly focuses on noble metals (Au, Ag, etc.), and research on non-precious metal single-atoms (Cu, Fe, etc.) is still relatively rare. Further exploration into more kinds of metal single atoms combined with different metal oxide substrate materials is expected to show surprising gas-sensitive effects. Secondly, most current studies focus on the impact of one-kind single metal atoms on gas sensing performance. However, using two different single metal atoms to develop bimetallic sites needs further exploration regarding the performance of metal oxide-based gas sensors.

(3) Some theoretical simulations have revealed that SACs enhance the gas-sensitizing performance by improving the charge transfer of interfaces. However, the effect of SACs on gas-sensitive performance varies with different coordination environments and local structures on the support materials, and the sensitization mechanism of SACs needs to be further clarified. The coordination of SACs on the support surface has a certain complexity, and synthesizing single-atom sites with specific local coordination environments and oxidation states is still challenging.

**Author Contributions:** Conceptualization, Y.Y.; formal analysis, Y.T.; investigation, Y.T., W.N., S.Z., J.H., H.L., C.H., P.Z., Y.W. and L.Z.; resources, W.N., S.Z., J.H., Y.S. and Y.D.; writing—original draft preparation, Y.Y.; writing—review and editing, B.D. and Y.H.; visualization, Y.S., Y.D., H.L. and C.H.; supervision, C.G., P.Z., Y.W., L.Z. and B.D.; project administration, Y.H.; funding acquisition, C.G. and Y.H. All authors have read and agreed to the published version of the manuscript.

**Funding:** This research was funded by the Natural Science Foundation of Chongqing (cstc2020jcsx-dxwtBX0052, CSTB2022NSCQ-LZX0075), the Fundamental Research Funds for Central Universities of China (2021CDJXDJH006, 2022CDJMRH-006 and 2023CDJXY-040), and the Key Laboratory of Gun Launch and Control Technology, NORINCO.

**Informed Consent Statement:** Not applicable.

**Data Availability Statement:** Not applicable.

**Conflicts of Interest:** The authors declare no conflicts of interest.

## References

1. Acosta, S.; Quintana, M. Chemically Functionalized 2D Transition Metal Dichalcogenides for Sensors. *Sensors* **2024**, *24*, 1817. [[CrossRef](#)]
2. Otero Vélez, C.; Flores, S.Y.; Fonseca, L.F.; Piñero Cruz, D.M. Palladium Phthalocyanine Nanowire-Based Highly Sensitive Sensors for NO<sub>2</sub>(g) Detection. *Sensors* **2024**, *24*, 1819. [[CrossRef](#)]
3. Flores, S.Y.; Gonzalez-Espiet, J.; Cintrón, J.; Villanueva, N.D.J.; Camino, F.E.; Kisslinger, K.; Cruz, D.M.P.; Rivera, R.D.; Fonseca, L.F. Fluorinated Iron and Cobalt Phthalocyanine Nanowire Chemiresistors for Environmental Gas Monitoring at Parts-per-Billion Levels. *ACS Appl. Nano Mater.* **2022**, *5*, 4688–4699. [[CrossRef](#)]
4. Jian, Y.; Zhang, N.; Liu, T.; Zhu, Y.; Wang, D.; Dong, H.; Guo, L.; Qu, D.; Jiang, X.; Du, T.; et al. Artificially Intelligent Olfaction for Fast and Noninvasive Diagnosis of Bladder Cancer from Urine. *ACS Sens.* **2022**, *7*, 1720–1731. [[CrossRef](#)]
5. Matsumoto, K.; Murakami, Y.; Shimizu, Y.; Hirayama, T.; Ishikawa, W.; Iwamura, M. Electronic Nose to Distinguish Bladder Cancer by Urinary Odour Feature: A Pilot Study. *Cancer Biomark.* **2020**, *28*, 33–39. [[CrossRef](#)]
6. Bruderer, T.; Gaisl, T.; Gaugg, M.T.; Nowak, N.; Streckenbach, B.; Müller, S.; Moeller, A.; Kohler, M.; Zenobi, R. On-Line Analysis of Exhaled Breath: Focus Review. *Chem. Rev.* **2019**, *119*, 10803–10828. [[CrossRef](#)]
7. Damdam, A.N.; Ozay, L.O.; Ozcan, C.K.; Alzahrani, A.; Helabi, R.; Salama, K.N. IoT-Enabled Electronic Nose System for Beef Quality Monitoring and Spoilage Detection. *Foods* **2023**, *12*, 2227. [[CrossRef](#)]
8. Banerjee, M.B.; Roy, R.B.; Tudu, B.; Bandyopadhyay, R.; Bhattacharyya, N. Black Tea Classification Employing Feature Fusion of E-Nose and E-Tongue Responses. *J. Food Eng.* **2019**, *244*, 55–63. [[CrossRef](#)]
9. Salinas, Y.; Ros-Lis, J.V.; Vivancos, J.-L.; Martínez-Mañez, R.; Marcos, M.D.; Aucejo, S.; Herranz, N.; Lorente, I.; Garcia, E. A Novel Colorimetric Sensor Array for Monitoring Fresh Pork Sausages Spoilage. *Food Control* **2014**, *35*, 166–176. [[CrossRef](#)]
10. Guo, L.; Wang, T.; Wu, Z.; Wang, J.; Wang, M.; Cui, Z.; Ji, S.; Cai, J.; Xu, C.; Chen, X. Portable Food-Freshness Prediction Platform Based on Colorimetric Barcode Combinatorics and Deep Convolutional Neural Networks. *Adv. Mater.* **2020**, *32*, 2004805. [[CrossRef](#)]
11. Kiani, S.; Minaei, S.; Ghasemi-Varnamkhasi, M. Application of Electronic Nose Systems for Assessing Quality of Medicinal and Aromatic Plant Products: A Review. *J. Appl. Res. Med. Aromat. Plants* **2016**, *3*, 1–9. [[CrossRef](#)]
12. Ray, M.; Ray, A.; Dash, S.; Mishra, A.; Achary, K.G.; Nayak, S.; Singh, S. Fungal Disease Detection in Plants: Traditional Assays, Novel Diagnostic Techniques and Biosensors. *Biosens. Bioelectron.* **2017**, *87*, 708–723. [[CrossRef](#)] [[PubMed](#)]
13. Maffei, M.E. Sites of Synthesis, Biochemistry and Functional Role of Plant Volatiles. *S. Afr. J. Bot.* **2010**, *76*, 612–631. [[CrossRef](#)]
14. Moseley, P.T. Progress in the Development of Semiconducting Metal Oxide Gas Sensors: A Review. *Meas. Sci. Technol.* **2017**, *28*, 082001. [[CrossRef](#)]
15. Gu, F.; Li, C.; Han, D.; Wang, Z. Manipulating the Defect Structure (V<sub>O</sub>) of In<sub>2</sub>O<sub>3</sub> Nanoparticles for Enhancement of Formaldehyde Detection. *ACS Appl. Mater. Interfaces* **2018**, *10*, 933–942. [[CrossRef](#)] [[PubMed](#)]
16. Al-Hashem, M.; Akbar, S.; Morris, P. Role of Oxygen Vacancies in Nanostructured Metal-Oxide Gas Sensors: A Review. *Sens. Actuators B Chem.* **2019**, *301*, 126845. [[CrossRef](#)]

17. Tischner, A.; Maier, T.; Stepper, C.; Köck, A. Ultrathin SnO<sub>2</sub> Gas Sensors Fabricated by Spray Pyrolysis for the Detection of Humidity and Carbon Monoxide. *Sens. Actuators B Chem.* **2008**, *134*, 796–802. [[CrossRef](#)]
18. Karbalaee Akbari, M.; Hai, Z.; Wei, Z.; Detavernier, C.; Solano, E.; Verpoort, F.; Zhuiykov, S. ALD-Developed Plasmonic Two-Dimensional Au–WO<sub>3</sub>–TiO<sub>2</sub> Heterojunction Architectonics for Design of Photovoltaic Devices. *ACS Appl. Mater. Interfaces* **2018**, *10*, 10304–10314. [[CrossRef](#)] [[PubMed](#)]
19. Peng, K.; Li, Q.; Ma, M.; Li, N.; Sheng, H.; Li, H.; Huang, Y.; Yun, F. Acidic Gas Determination Using Indium Tin Oxide-Based Gas Sensors. *Sensors* **2024**, *24*, 1286. [[CrossRef](#)]
20. Santos-Betancourt, A.; Santos-Ceballos, J.C.; Alouani, M.A.; Malik, S.B.; Romero, A.; Ramírez, J.L.; Vilanova, X.; Llobet, E. ZnO Decorated Graphene-Based NFC Tag for Personal NO<sub>2</sub> Exposure Monitoring during a Workday. *Sensors* **2024**, *24*, 1431. [[CrossRef](#)]
21. Sun, G.; Chen, H.; Li, Y.; Chen, Z.; Zhang, S.; Ma, G.; Jia, T.; Cao, J.; Bala, H.; Wang, X.; et al. Synthesis and Improved Gas Sensing Properties of NiO-Decorated SnO<sub>2</sub> Microflowers Assembled with Porous Nanorods. *Sens. Actuators B Chem.* **2016**, *233*, 180–192. [[CrossRef](#)]
22. Navale, S.; Shahbaz, M.; Mirzaei, A.; Kim, S.S.; Kim, H.W. Effect of Ag Addition on the Gas-Sensing Properties of Nanostructured Resistive-Based Gas Sensors: An Overview. *Sensors* **2021**, *21*, 6454. [[CrossRef](#)] [[PubMed](#)]
23. Lee, J.; Jung, Y.; Sung, S.-H.; Lee, G.; Kim, J.; Seong, J.; Shim, Y.-S.; Jun, S.C.; Jeon, S. High-Performance Gas Sensor Array for Indoor Air Quality Monitoring: The Role of Au Nanoparticles on WO<sub>3</sub>, SnO<sub>2</sub>, and NiO-Based Gas Sensors. *J. Mater. Chem. A* **2021**, *9*, 1159–1167. [[CrossRef](#)]
24. Zhu, L.-Y.; Ou, L.-X.; Mao, L.-W.; Wu, X.-Y.; Liu, Y.-P.; Lu, H.-L. Advances in Noble Metal-Decorated Metal Oxide Nanomaterials for Chemiresistive Gas Sensors: Overview. *Nano-Micro Lett.* **2023**, *15*, 89. [[CrossRef](#)]
25. Bahrami, B.; Khodadadi, A.; Kazemeini, M.; Mortazavi, Y. Enhanced CO Sensitivity and Selectivity of Gold Nanoparticles-Doped SnO<sub>2</sub> Sensor in Presence of Propane and Methane. *Sens. Actuators B Chem.* **2008**, *133*, 352–356. [[CrossRef](#)]
26. Y Nishchakova, A.D.; Bulusheva, L.G.; Bulushev, D.A. Supported Ni Single-Atom Catalysts: Synthesis, Structure, and Applications in Thermocatalytic Reactions. *Catalysts* **2023**, *13*, 845. [[CrossRef](#)]
27. Flytzani-Stephanopoulos, M.; Gates, B.C. Atomically Dispersed Supported Metal Catalysts. *Annu. Rev. Chem. Biomol. Eng.* **2012**, *3*, 545–574. [[CrossRef](#)] [[PubMed](#)]
28. Sun, T.; Xu, L.; Wang, D.; Li, Y. Metal Organic Frameworks Derived Single Atom Catalysts for Electrocatalytic Energy Conversion. *Nano Res.* **2019**, *12*, 2067–2080. [[CrossRef](#)]
29. Cai, Y.; Bai, Z.; Chintalapati, S.; Zeng, Q.; Feng, Y.P. Transition Metal Atoms Pathways on Rutile TiO<sub>2</sub> (110) Surface: Distribution of Ti<sup>3+</sup> States and Evidence of Enhanced Peripheral Charge Accumulation. *J. Chem. Phys.* **2013**, *138*, 154711. [[CrossRef](#)]
30. Zhang, J.; Zhao, Y.; Guo, X.; Chen, C.; Dong, C.-L.; Liu, R.-S.; Han, C.-P.; Li, Y.; Gogotsi, Y.; Wang, G. Single Platinum Atoms Immobilized on an MXene as an Efficient Catalyst for the Hydrogen Evolution Reaction. *Nat. Catal.* **2018**, *1*, 985–992. [[CrossRef](#)]
31. Wei, H.; Liu, X.; Wang, A.; Zhang, L.; Qiao, B.; Yang, X.; Huang, Y.; Miao, S.; Liu, J.; Zhang, T. FeO<sub>x</sub>-Supported Platinum Single-Atom and Pseudo-Single-Atom Catalysts for Chemoselective Hydrogenation of Functionalized Nitroarenes. *Nat. Commun.* **2014**, *5*, 5634. [[CrossRef](#)] [[PubMed](#)]
32. Kyriakou, G.; Boucher, M.B.; Jewell, A.D.; Lewis, E.A.; Lawton, T.J.; Baber, A.E.; Tierney, H.L.; Flytzani-Stephanopoulos, M.; Sykes, E.C.H. Isolated Metal Atom Geometries as a Strategy for Selective Heterogeneous Hydrogenations. *Science* **2012**, *335*, 1209–1212. [[CrossRef](#)] [[PubMed](#)]
33. Lei, G.; Pan, H.; Mei, H.; Liu, X.; Lu, G.; Lou, C.; Li, Z.; Zhang, J. Emerging Single Atom Catalysts in Gas Sensors. *Chem. Soc. Rev.* **2022**, *51*, 7260–7280. [[CrossRef](#)] [[PubMed](#)]
34. Chu, T.; Rong, C.; Zhou, L.; Mao, X.; Zhang, B.; Xuan, F. Progress and Perspectives of Single-Atom Catalysts for Gas Sensing. *Adv. Mater.* **2023**, *35*, 2206783. [[CrossRef](#)] [[PubMed](#)]
35. Lu, J.; Elam, J.W.; Stair, P.C. Synthesis and Stabilization of Supported Metal Catalysts by Atomic Layer Deposition. *Acc. Chem. Res.* **2013**, *46*, 1806–1815. [[CrossRef](#)] [[PubMed](#)]
36. Fonseca, J.; Lu, J. Single-Atom Catalysts Designed and Prepared by the Atomic Layer Deposition Technique. *ACS Catal.* **2021**, *11*, 7018–7059. [[CrossRef](#)]
37. Lu, J.; Elam, J.W.; Stair, P.C. Atomic Layer Deposition—Sequential Self-Limiting Surface Reactions for Advanced Catalyst “Bottom-up” Synthesis. *Surf. Sci. Rep.* **2016**, *71*, 410–472. [[CrossRef](#)]
38. Zhao, C.; Tang, Y.; Yu, C.; Tan, X.; Banis, M.N.; Li, S.; Wan, G.; Huang, H.; Zhang, L.; Yang, H.; et al. Insights into the Electronic Origin of Enhancing the Catalytic Activity of Co<sub>3</sub>O<sub>4</sub> for Oxygen Evolution by Single Atom Ruthenium. *Nano Today* **2020**, *34*, 100955. [[CrossRef](#)]
39. Wang, X.; Jin, B.; Jin, Y.; Wu, T.; Ma, L.; Liang, X. Supported Single Fe Atoms Prepared via Atomic Layer Deposition for Catalytic Reactions. *ACS Appl. Nano Mater.* **2020**, *3*, 2867–2874. [[CrossRef](#)]
40. Zhang, L.; Banis, M.N.; Sun, X. Single-Atom Catalysts by the Atomic Layer Deposition Technique. *Natl. Sci. Rev.* **2018**, *5*, 628–630. [[CrossRef](#)]
41. Wang, L.; Huang, L.; Liang, F.; Liu, S.; Wang, Y.; Zhang, H. Preparation, Characterization and Catalytic Performance of Single-Atom Catalysts. *Chin. J. Catal.* **2017**, *38*, 1528–1539. [[CrossRef](#)]
42. Wang, N.; Sun, Q.; Zhang, T.; Mayoral, A.; Li, L.; Zhou, X.; Xu, J.; Zhang, P.; Yu, J. Impregnating Subnanometer Metallic Nanocatalysts into Self-Pillared Zeolite Nanosheets. *J. Am. Chem. Soc.* **2021**, *143*, 6905–6914. [[CrossRef](#)] [[PubMed](#)]

43. Zhang, Z.; Liu, J.; Wang, J.; Wang, Q.; Wang, Y.; Wang, K.; Wang, Z.; Gu, M.; Tang, Z.; Lim, J.; et al. Single-Atom Catalyst for High-Performance Methanol Oxidation. *Nat. Commun.* **2021**, *12*, 5235. [[CrossRef](#)] [[PubMed](#)]
44. Xiong, H.; Datye, A.K.; Wang, Y. Thermally Stable Single-Atom Heterogeneous Catalysts. *Adv. Mater.* **2021**, *33*, 2004319. [[CrossRef](#)]
45. Hai, X.; Xi, S.; Mitchell, S.; Harrath, K.; Xu, H.; Akl, D.F.; Kong, D.; Li, J.; Li, Z.; Sun, T.; et al. Scalable Two-Step Annealing Method for Preparing Ultra-High-Density Single-Atom Catalyst Libraries. *Nat. Nanotechnol.* **2022**, *17*, 174–181. [[CrossRef](#)]
46. Li, W.; Guo, Z.; Yang, J.; Li, Y.; Sun, X.; He, H.; Li, S.; Zhang, J. Advanced Strategies for Stabilizing Single-Atom Catalysts for Energy Storage and Conversion. *Electrochem. Energy Rev.* **2022**, *5*, 9. [[CrossRef](#)]
47. Millet, M.-M.; Algara-Siller, G.; Wrabetz, S.; Mazheika, A.; Girgsdies, F.; Teschner, D.; Seitz, F.; Tarasov, A.; Levchenko, S.V.; Schlögl, R.; et al. Ni Single Atom Catalysts for CO<sub>2</sub> Activation. *J. Am. Chem. Soc.* **2019**, *141*, 2451–2461. [[CrossRef](#)] [[PubMed](#)]
48. Shah, K.; Dai, R.; Mateen, M.; Hassan, Z.; Zhuang, Z.; Liu, C.; Israr, M.; Cheong, W.-C.; Hu, B.; Tu, R.; et al. Cobalt Single Atom Incorporated in Ruthenium Oxide Sphere: A Robust Bifunctional Electrocatalyst for HER and OER. *Angew. Chem. Int. Ed.* **2022**, *61*, e202114951. [[CrossRef](#)] [[PubMed](#)]
49. Gu, H.; Liu, X.; Liu, X.; Ling, C.; Wei, K.; Zhan, G.; Guo, Y.; Zhang, L. Adjacent single-atom irons boosting molecular oxygen activation on MnO. *Nat. Commun.* **2021**, *12*, 5422. [[CrossRef](#)]
50. Li, Z.; Wang, D.; Wu, Y.; Li, Y. Recent Advances in the Precise Control of Isolated Single-Site Catalysts by Chemical Methods. *Natl. Sci. Rev.* **2018**, *5*, 673–689. [[CrossRef](#)]
51. Liu, P.; Zhao, Y.; Qin, R.; Mo, S.; Chen, G.; Gu, L.; Chevrier, D.M.; Zhang, P.; Guo, Q.; Zang, D.; et al. Photochemical Route for Synthesizing Atomically Dispersed Palladium Catalysts. *Science* **2016**, *352*, 797–800. [[CrossRef](#)] [[PubMed](#)]
52. Wei, H.; Huang, K.; Wang, D.; Zhang, R.; Ge, B.; Ma, J.; Wen, B.; Zhang, S.; Li, Q.; Lei, M.; et al. Iced Photochemical Reduction to Synthesize Atomically Dispersed Metals by Suppressing Nanocrystal Growth. *Nat. Commun.* **2017**, *8*, 1490. [[CrossRef](#)] [[PubMed](#)]
53. Shi, Q.; Fu, S.; Zhu, C.; Song, J.; Du, D.; Lin, Y. Metal–Organic Frameworks-Based Catalysts for Electrochemical Oxygen Evolution. *Mater. Horiz.* **2019**, *6*, 684–702. [[CrossRef](#)]
54. Yin, P.; Yao, T.; Wu, Y.; Zheng, L.; Lin, Y.; Liu, W.; Ju, H.; Zhu, J.; Hong, X.; Deng, Z.; et al. Single Cobalt Atoms with Precise N-Coordination as Superior Oxygen Reduction Reaction Catalysts. *Angew. Chem.* **2016**, *128*, 10958–10963. [[CrossRef](#)]
55. Wang, J.; Han, G.; Wang, L.; Du, L.; Chen, G.; Gao, Y.; Ma, Y.; Du, C.; Cheng, X.; Zuo, P.; et al. ZIF-8 with Ferrocene Encapsulated: A Promising Precursor to Single-Atom Fe Embedded Nitrogen-Doped Carbon as Highly Efficient Catalyst for Oxygen Electroreduction. *Small* **2018**, *14*, 1704282. [[CrossRef](#)] [[PubMed](#)]
56. Liu, B.; Zhang, L.; Luo, Y.; Gao, L.; Duan, G. The Dehydrogenation of H-S Bond into Sulfur Species on Supported Pd Single Atoms Allows Highly Selective and Sensitive Hydrogen Sulfide Detection. *Small* **2021**, *17*, 2105643. [[CrossRef](#)] [[PubMed](#)]
57. Rice, S.B.; Koo, J.Y.; Disko, M.M.; Treacy, M.M.J. On the Imaging of Pt Atoms in Zeolite Frameworks. *Ultramicroscopy* **1990**, *34*, 108–118. [[CrossRef](#)]
58. Besenbacher, F.; Brorson, M.; Clausen, B.S.; Helveg, S.; Hinnemann, B.; Kibsgaard, J.; Lauritsen, J.V.; Moses, P.G.; Nørskov, J.K.; Topsøe, H. Recent STM, DFT and HAADF-STEM Studies of Sulfide-Based Hydrotreating Catalysts: Insight into Mechanistic, Structural and Particle Size Effects. *Catal. Today* **2008**, *130*, 86–96. [[CrossRef](#)]
59. Gu, W.; Pei, A.; Zhang, S.; Jiang, F.; Jia, Y.; Qin, Q.; Du, R.; Li, Z.; Liu, R.; Qiu, Y.; et al. Atomic-Interface Effect of Single-Atom Ru/CoO<sub>x</sub> for Selective Electrooxidation of 5-Hydroxymethylfurfural. *ACS Appl. Mater. Interfaces* **2023**, *15*, 28036–28043. [[CrossRef](#)]
60. Wang, Y.; Hong, G.; Zhang, Y.; Liu, Y.; Cen, W.; Wang, L.; Wu, Z. Photocatalytic Oxidative Coupling of Methane over Au<sub>1</sub>Ag Single-Atom Alloy Modified ZnO with Oxygen and Water Vapor: Synergy of Gold and Silver. *Angew. Chem. Int. Ed.* **2023**, *62*, e202310525. [[CrossRef](#)]
61. Marcinkowski, M.D.; Darby, M.T.; Liu, J.; Wimple, J.M.; Lucci, F.R.; Lee, S.; Michaelides, A.; Flytzani-Stephanopoulos, M.; Stamatakis, M.; Sykes, E.C.H. Pt/Cu Single-Atom Alloys as Coke-Resistant Catalysts for Efficient C–H Activation. *Nat. Chem.* **2018**, *10*, 325–332. [[CrossRef](#)]
62. Barbara, S. *Probing Active Sites of Heterogeneous Catalysts by X-ray Absorption Spectroscopy*; University of California: Santa Barbara, CA, USA, 2021.
63. Oikawa, T.; Ookoshi, T.; Tanaka, T.; Yamamoto, T.; Onaka, M. A New Heterogeneous Olefin Metathesis Catalyst Composed of Rhenium Oxide and Mesoporous Alumina. *Microporous Mesoporous Mater.* **2004**, *74*, 93–103. [[CrossRef](#)]
64. Xu, T.; Zheng, H.; Zhang, P. Isolated Pt Single Atomic Sites Anchored on Nanoporous TiO<sub>2</sub> Film for Highly Efficient Photocatalytic Degradation of Low Concentration Toluene. *J. Hazard. Mater.* **2020**, *388*, 121746. [[CrossRef](#)]
65. Huang, Z.; Zhang, J.; Du, Y.; Zhang, Y.; Wu, X.; Jing, G. Self-assembly of Atomically Dispersed Ag Catalysts on Polyhedral Co<sub>3</sub>O<sub>4</sub> at Elevated Temperatures: A Top-Down Nanofabrication of High-Loading Atomically Dispersed Catalysts. *ChemCatChem* **2020**, *12*, 561–568. [[CrossRef](#)]
66. Che, M.; Védrine, J.C. (Eds.) *Characterization of Solid Materials and Heterogeneous Catalysts: From Structure to Surface Reactivity*, 1st ed.; Wiley: Hoboken, NJ, USA, 2012; ISBN 978-3-527-32687-7.
67. Rodríguez, J.A.; Hanson, J.C.; Chupas, P.J. (Eds.) *In-Situ Characterization of Heterogeneous Catalysts*; Wiley: Hoboken, NJ, USA, 2013; ISBN 978-1-118-00016-8.
68. Lamberti, C.; Zecchina, A.; Groppo, E.; Bordiga, S. Probing the Surfaces of Heterogeneous Catalysts by in Situ IR Spectroscopy. *Chem. Soc. Rev.* **2010**, *39*, 4951. [[CrossRef](#)] [[PubMed](#)]
69. Zaera, F. New Advances in the Use of Infrared Absorption Spectroscopy for the Characterization of Heterogeneous Catalytic Reactions. *Chem. Soc. Rev.* **2014**, *43*, 7624–7663. [[CrossRef](#)]

70. Lang, R.; Du, X.; Huang, Y.; Jiang, X.; Zhang, Q.; Guo, Y.; Liu, K.; Qiao, B.; Wang, A.; Zhang, T. Single-Atom Catalysts Based on the Metal–Oxide Interaction. *Chem. Rev.* **2020**, *120*, 11986–12043. [[CrossRef](#)] [[PubMed](#)]
71. Qiao, B.; Wang, A.; Yang, X.; Allard, L.F.; Jiang, Z.; Cui, Y.; Liu, J.; Li, J.; Zhang, T. Single-Atom Catalysis of CO Oxidation Using Pt<sub>1</sub>/FeOx. *Nat. Chem.* **2011**, *3*, 634–641. [[CrossRef](#)] [[PubMed](#)]
72. Yan, D.; Chen, J.; Jia, H. Temperature-Induced Structure Reconstruction to Prepare a Thermally Stable Single-Atom Platinum Catalyst. *Angew. Chem. Int. Ed.* **2020**, *59*, 13562–13567. [[CrossRef](#)]
73. Liu, L.; Corma, A. Metal Catalysts for Heterogeneous Catalysis: From Single Atoms to Nanoclusters and Nanoparticles. *Chem. Rev.* **2018**, *118*, 4981–5079. [[CrossRef](#)]
74. Matsubu, J.C.; Zhang, S.; DeRita, L.; Marinkovic, N.S.; Chen, J.G.; Graham, G.W.; Pan, X.; Christopher, P. Adsorbate-Mediated Strong Metal–Support Interactions in Oxide-Supported Rh Catalysts. *Nat. Chem.* **2017**, *9*, 120–127. [[CrossRef](#)] [[PubMed](#)]
75. Tauster, S.J.; Fung, S.C.; Garten, R.L. Strong Metal–Support Interactions. Group 8 Noble Metals Supported on Titanium Dioxide. *J. Am. Chem. Soc.* **1978**, *100*, 170–175. [[CrossRef](#)]
76. Han, B.; Guo, Y.; Huang, Y.; Xi, W.; Xu, J.; Luo, J.; Qi, H.; Ren, Y.; Liu, X.; Qiao, B.; et al. Strong Metal–Support Interactions between Pt Single Atoms and TiO. *Angew. Chem. Int. Ed.* **2020**, *59*, 11824–11829. [[CrossRef](#)] [[PubMed](#)]
77. Tian, H.; Cui, X.; Zeng, L.; Su, L.; Song, Y.; Shi, J. Oxygen Vacancy-Assisted Hydrogen Evolution Reaction of the Pt/WO<sub>3</sub> Electrocatalyst. *J. Mater. Chem. A* **2019**, *7*, 6285–6293. [[CrossRef](#)]
78. Wu, J.; Wu, Y.; Lu, L.; Zhang, D.; Wang, X. Single-Atom Au Catalyst Loaded on CeO<sub>2</sub>: A Novel Single-Atom Nanozyme Electrochemical H<sub>2</sub>O<sub>2</sub> Sensor. *Talanta Open* **2021**, *4*, 100075. [[CrossRef](#)]
79. Duan, S.; Wang, R.; Liu, J. Stability Investigation of a High Number Density Pt<sub>1</sub>/Fe<sub>2</sub>O<sub>3</sub> Single-Atom Catalyst under Different Gas Environments by HAADF-STEM. *Nanotechnology* **2018**, *29*, 204002. [[CrossRef](#)] [[PubMed](#)]
80. Gu, X.-K.; Qiao, B.; Huang, C.-Q.; Ding, W.-C.; Sun, K.; Zhan, E.; Zhang, T.; Liu, J.; Li, W.-X. Supported Single Pt<sub>1</sub>/Au<sub>1</sub> Atoms for Methanol Steam Reforming. *ACS Catal.* **2014**, *4*, 3886–3890. [[CrossRef](#)]
81. Sanchez, M. Oxygen Vacancy Model in Strong Metal–Support Interaction. *J. Catal.* **1987**, *104*, 120–135. [[CrossRef](#)]
82. Wan, J.; Chen, W.; Jia, C.; Zheng, L.; Dong, J.; Zheng, X.; Wang, Y.; Yan, W.; Chen, C.; Peng, Q.; et al. Defect Effects on TiO<sub>2</sub> Nanosheets: Stabilizing Single Atomic Site Au and Promoting Catalytic Properties. *Adv. Mater.* **2018**, *30*, 1705369. [[CrossRef](#)]
83. Zhang, S.; Nguyen, L.; Liang, J.-X.; Shan, J.; Liu, J.; Frenkel, A.I.; Patlolla, A.; Huang, W.; Li, J.; Tao, F. Catalysis on Singly Dispersed Bimetallic Sites. *Nat. Commun.* **2015**, *6*, 7938. [[CrossRef](#)]
84. Chang, T.-Y.; Tanaka, Y.; Ishikawa, R.; Toyoura, K.; Matsunaga, K.; Ikuhara, Y.; Shibata, N. Direct Imaging of Pt Single Atoms Adsorbed on TiO<sub>2</sub> (110) Surfaces. *Nano Lett.* **2014**, *14*, 134–138. [[CrossRef](#)] [[PubMed](#)]
85. Qu, W.; Liu, X.; Chen, J.; Dong, Y.; Tang, X.; Chen, Y. Single-Atom Catalysts Reveal the Dinuclear Characteristic of Active Sites in NO Selective Reduction with NH. *Nat. Commun.* **2020**, *11*, 1532. [[CrossRef](#)] [[PubMed](#)]
86. Kwak, J.H.; Hu, J.; Mei, D.; Yi, C.-W.; Kim, D.H.; Peden, C.H.F.; Allard, L.F.; Szanyi, J. Coordinatively Unsaturated Al<sup>3+</sup> Centers as Binding Sites for Active Catalyst Phases of Platinum on  $\gamma$ -Al<sub>2</sub>O. *Science* **2009**, *325*, 1670–1673. [[CrossRef](#)] [[PubMed](#)]
87. Qi, K.; Cui, X.; Gu, L.; Yu, S.; Fan, X.; Luo, M.; Xu, S.; Li, N.; Zheng, L.; Zhang, Q.; et al. Single-Atom Cobalt Array Bound to Distorted 1T MoS<sub>2</sub> with Ensemble Effect for Hydrogen Evolution Catalysis. *Nat. Commun.* **2019**, *10*, 5231. [[CrossRef](#)] [[PubMed](#)]
88. Heemeier, M.; Frank, M.; Libuda, J.; Wolter, K.; Kuhlenbeck, H.; Baumer, M. The Influence of OH Groups on the Growth of Rhodium on Alumina: A Model Study. *Catal. Lett.* **2000**, *68*, 19–24. [[CrossRef](#)]
89. Wang, F.; Ma, J.; Xin, S.; Wang, Q.; Xu, J.; Zhang, C.; He, H.; Cheng Zeng, X. Resolving the Puzzle of Single-Atom Silver Dispersion on Nanosized  $\gamma$ -Al<sub>2</sub>O<sub>3</sub> Surface for High Catalytic Performance. *Nat. Commun.* **2020**, *11*, 529. [[CrossRef](#)] [[PubMed](#)]
90. Yang, M.; Li, S.; Wang, Y.; Herron, J.A.; Xu, Y.; Allard, L.F.; Lee, S.; Huang, J.; Mavrikakis, M.; Flytzani-Stephanopoulos, M. Catalytically Active Au–O(OH)<sub>x</sub>—Species Stabilized by Alkali Ions on Zeolites and Mesoporous Oxides. *Science* **2014**, *346*, 1498–1501. [[CrossRef](#)] [[PubMed](#)]
91. Yang, M.; Liu, J.; Lee, S.; Zugic, B.; Huang, J.; Allard, L.F.; Flytzani-Stephanopoulos, M. A Common Single-Site Pt(II)–O(OH)<sub>x</sub>—Species Stabilized by Sodium on “Active” and “Inert” Supports Catalyzes the Water-Gas Shift Reaction. *J. Am. Chem. Soc.* **2015**, *137*, 3470–3473. [[CrossRef](#)]
92. Kuai, L.; Chen, Z.; Liu, S.; Kan, E.; Yu, N.; Ren, Y.; Fang, C.; Li, X.; Li, Y.; Geng, B. Titania Supported Synergistic Palladium Single Atoms and Nanoparticles for Room Temperature Ketone and Aldehydes Hydrogenation. *Nat. Commun.* **2020**, *11*, 48. [[CrossRef](#)]
93. Zhang, Z.; Zhu, Y.; Asakura, H.; Zhang, B.; Zhang, J.; Zhou, M.; Han, Y.; Tanaka, T.; Wang, A.; Zhang, T.; et al. Thermally Stable Single Atom Pt/m-Al<sub>2</sub>O<sub>3</sub> for Selective Hydrogenation and CO Oxidation. *Nat. Commun.* **2017**, *8*, 16100. [[CrossRef](#)]
94. Yang, K.; Liu, Y.; Deng, J.; Zhao, X.; Yang, J.; Han, Z.; Hou, Z.; Dai, H. Three-Dimensionally Ordered Mesoporous Iron Oxide-Supported Single-Atom Platinum: Highly Active Catalysts for Benzene Combustion. *Appl. Catal. B Environ.* **2019**, *244*, 650–659. [[CrossRef](#)]
95. Azofra, L.M.; Morlanés, N.; Poater, A.; Samantaray, M.K.; Vidjayacoumar, B.; Albahily, K.; Cavallo, L.; Basset, J. Single-Site Molybdenum on Solid Support Materials for Catalytic Hydrogenation of N<sub>2</sub>-into-NH. *Angew. Chem. Int. Ed.* **2018**, *57*, 15812–15816. [[CrossRef](#)]
96. De, S.; Babak, M.V.; Hülsey, M.J.; Ang, W.H.; Yan, N. Designed Precursor for the Controlled Synthesis of Highly Active Atomic and Sub-nanometric Platinum Catalysts on Mesoporous Silica. *Chem. Asian J.* **2018**, *13*, 1053–1059. [[CrossRef](#)]
97. Kosinov, N.; Liu, C.; Hensen, E.J.M.; Pidko, E.A. Engineering of Transition Metal Catalysts Confined in Zeolites. *Chem. Mater.* **2018**, *30*, 3177–3198. [[CrossRef](#)]

98. Liu, L.; Corma, A. Evolution of Isolated Atoms and Clusters in Catalysis. *Trends Chem.* **2020**, *2*, 383–400. [[CrossRef](#)]
99. Ye, T.-N.; Xiao, Z.; Li, J.; Gong, Y.; Abe, H.; Niwa, Y.; Sasase, M.; Kitano, M.; Hosono, H. Stable Single Platinum Atoms Trapped in Sub-Nanometer Cavities in  $12\text{CaO}\cdot 7\text{Al}_2\text{O}_3$  for Chemoselective Hydrogenation of Nitroarenes. *Nat. Commun.* **2020**, *11*, 1020. [[CrossRef](#)]
100. Shin, H.; Jung, W.-G.; Kim, D.-H.; Jang, J.-S.; Kim, Y.H.; Koo, W.-T.; Bae, J.; Park, C.; Cho, S.-H.; Kim, B.J.; et al. Single-Atom Pt Stabilized on One-Dimensional Nanostructure Support via Carbon Nitride/ $\text{SnO}_2$  Heterojunction Trapping. *ACS Nano* **2020**, *14*, 11394–11405. [[CrossRef](#)]
101. Kumar, R.; Kumar, M. Single-Atom Catalysts Boosted Ultrathin Film Sensors. *Rare Met.* **2020**, *39*, 1110–1112. [[CrossRef](#)]
102. Zhou, L.; Chang, X.; Zheng, W.; Liu, X.; Zhang, J. Single Atom Rh-Sensitized  $\text{SnO}_2$  via Atomic Layer Deposition for Efficient Formaldehyde Detection. *Chem. Eng. J.* **2023**, *475*, 146300. [[CrossRef](#)]
103. Sun, L.; Wang, B.; Wang, Y. High-Temperature Gas Sensor Based on Novel Pt Single Atoms@ $\text{SnO}_2$  Nanorods@SiC Nanosheets Multi-Heterojunctions. *ACS Appl. Mater. Interfaces* **2020**, *12*, 21808–21817. [[CrossRef](#)]
104. Lu, Z.; Meng, S.; Ma, Z.; Yang, M.; Ma, D.; Yang, Z.; Talib, S.H. Electronic and Catalytic Properties of Ti Single atoms@ $\text{SnO}_2$  and Its Implications on Sensing Mechanism for CO. *Appl. Surf. Sci.* **2022**, *594*, 153500. [[CrossRef](#)]
105. Degler, D.; Müller, S.A.; Doronkin, D.E.; Wang, D.; Grunwaldt, J.-D.; Weimar, U.; Barsan, N. Platinum Loaded Tin Dioxide: A Model System for Unravelling the Interplay between Heterogeneous Catalysis and Gas Sensing. *J. Mater. Chem. A* **2018**, *6*, 2034–2046. [[CrossRef](#)]
106. Degler, D.; Pereira De Carvalho, H.W.; Kvashnina, K.; Grunwaldt, J.-D.; Weimar, U.; Barsan, N. Structure and Chemistry of Surface-Doped Pt: $\text{SnO}_2$  Gas Sensing Materials. *RSC Adv.* **2016**, *6*, 28149–28155. [[CrossRef](#)]
107. Xu, Y.; Zheng, W.; Liu, X.; Zhang, L.; Zheng, L.; Yang, C.; Pinna, N.; Zhang, J. Platinum Single Atoms on Tin Oxide Ultrathin Films for Extremely Sensitive Gas Detection. *Mater. Horiz.* **2020**, *7*, 1519–1527. [[CrossRef](#)]
108. Liu, L.; Zhou, P.; Su, X.; Liu, Y.; Sun, Y.; Yang, H.; Fu, H.; Qu, X.; Liu, S.; Zheng, S. Synergistic Ni Single Atoms and Oxygen Vacancies on  $\text{SnO}_2$  Nanorods toward Promoting  $\text{SO}_2$  Gas Sensing. *Sens. Actuators B Chem.* **2022**, *351*, 130983. [[CrossRef](#)]
109. Shin, H.; Ko, J.; Park, C.; Kim, D.; Ahn, J.; Jang, J.; Kim, Y.H.; Cho, S.; Baik, H.; Kim, I. Sacrificial Template-Assisted Synthesis of Inorganic Nanosheets with High-Loading Single-Atom Catalysts: A General Approach. *Adv. Funct. Mater.* **2022**, *32*, 2110485. [[CrossRef](#)]
110. Wang, P.; Guo, S.; Hu, Z.; Zhou, L.; Li, T.; Pu, S.; Mao, H.; Cai, H.; Zhu, Z.; Chen, B.; et al. Single-Atom Cu Stabilized on Ultrathin  $\text{WO}_{2.72}$  Nanowire for Highly Selective and Ultrasensitive ppb-Level Toluene Detection. *Adv. Sci.* **2023**, *10*, 2302778. [[CrossRef](#)]
111. Gu, F.; Cui, Y.; Han, D.; Hong, S.; Flytzani-Stephanopoulos, M.; Wang, Z. Atomically Dispersed Pt (II) on  $\text{WO}_3$  for Highly Selective Sensing and Catalytic Oxidation of Triethylamine. *Appl. Catal. B Environ.* **2019**, *256*, 117809. [[CrossRef](#)]
112. Yuan, T.; Xue, Z.; Chen, Y.; Xu, J. Single Pt Atom-Based Gas Sensor: Break the Detection Limit and Selectivity of Acetone. *Sens. Actuators B Chem.* **2023**, *397*, 134139. [[CrossRef](#)]
113. Zeng, J.; Rong, Q.; Xiao, B.; Yu, R.; Zi, B.; Kuang, X.; Deng, X.; Ma, Y.; Zhang, J.; Wu, J.; et al. Single-Atom Silver Loaded on Tungsten Oxide with Oxygen Vacancies for High Performance Triethylamine Gas Sensors. *J. Mater. Chem. A* **2021**, *9*, 8704–8710. [[CrossRef](#)]
114. Gu, F.; Luo, C.; Han, D.; Hong, S.; Wang, Z. Atomically Dispersed Pt on 3DOM  $\text{WO}_3$  Promoted with Cobalt and Nickel Oxides for Highly Selective and Highly Sensitive Detection of Xylene. *Sens. Actuators B Chem.* **2019**, *297*, 126772. [[CrossRef](#)]
115. Wang, C.; Xie, J.; Chang, X.; Zheng, W.; Zhang, J.; Liu, X. ZnO Single Nanowire Gas Sensor: A Platform to Investigate the Sensitization of Pt. *Chem. Eng. J.* **2023**, *473*, 145481. [[CrossRef](#)]
116. Xue, Z.; Yan, M.; Yu, X.; Tong, Y.; Zhou, H.; Zhao, Y.; Wang, Z.; Zhang, Y.; Xiong, C.; Yang, J.; et al. One-Dimensional Segregated Single Au Sites on Step-Rich ZnO Ladder for Ultrasensitive  $\text{NO}_2$  Sensors. *Chem* **2020**, *6*, 3364–3373. [[CrossRef](#)]
117. Liu, L.; Mao, C.; Fu, H.; Qu, X.; Zheng, S. ZnO Nanorod-Immobilized Pt Single-Atoms as an Ultrasensitive Sensor for Triethylamine Detection. *ACS Appl. Mater. Interfaces* **2023**, *15*, 16654–16663. [[CrossRef](#)]
118. Rong, Q.; Xiao, B.; Zeng, J.; Yu, R.; Zi, B.; Zhang, G.; Zhu, Z.; Zhang, J.; Wu, J.; Liu, Q. Pt Single Atom-Induced Activation Energy and Adsorption Enhancement for an Ultrasensitive Ppb-Level Methanol Gas Sensor. *ACS Sens.* **2022**, *7*, 199–206. [[CrossRef](#)]
119. Gu, F.; Di, M.; Han, D.; Hong, S.; Wang, Z. Atomically Dispersed Au on  $\text{In}_2\text{O}_3$  Nanosheets for Highly Sensitive and Selective Detection of Formaldehyde. *ACS Sens.* **2020**, *5*, 2611–2619. [[CrossRef](#)]
120. Li, D.; Li, Y.; Wang, X.; Sun, G.; Cao, J.; Wang, Y. Surface Modification of  $\text{In}_2\text{O}_3$  Porous Nanospheres with Au Single Atoms for Ultrafast and Highly Sensitive Detection of CO. *Appl. Surf. Sci.* **2023**, *613*, 155987. [[CrossRef](#)]
121. Gu, F.; Su, Y.; Hong, S.; Wang, J.; Wang, P.; Han, D.; Wang, Z.; Qiao, Z.; Hu, Y. Effects of Hydrogen Treatment on the Triethylamine-Sensing Properties of the Platinum-Loaded  $\text{In}_2\text{O}_3$  Nanosheets. *Sens. Actuators B Chem.* **2022**, *372*, 132632. [[CrossRef](#)]
122. Li, Q.; Li, Z.; Zhang, Q.; Zheng, L.; Yan, W.; Liang, X.; Gu, L.; Chen, C.; Wang, D.; Peng, Q.; et al. Porous  $\gamma\text{-Fe}_2\text{O}_3$  Nanoparticle Decorated with Atomically Dispersed Platinum: Study on Atomic Site Structural Change and Gas Sensor Activity Evolution. *Nano Res.* **2021**, *14*, 1435–1442. [[CrossRef](#)]
123. Ye, X.-L.; Lin, S.-J.; Zhang, J.-W.; Jiang, H.-J.; Cao, L.-A.; Wen, Y.-Y.; Yao, M.-S.; Li, W.-H.; Wang, G.-E.; Xu, G. Boosting Room Temperature Sensing Performances by Atomically Dispersed Pd Stabilized via Surface Coordination. *ACS Sens.* **2021**, *6*, 1103–1110. [[CrossRef](#)]
124. Koga, K. Electronic and Catalytic Effects of Single-Atom Pd Additives on the Hydrogen Sensing Properties of  $\text{Co}_3\text{O}_4$  Nanoparticle Films. *ACS Appl. Mater. Interfaces* **2020**, *12*, 20806–20823. [[CrossRef](#)] [[PubMed](#)]

125. Hu, J.; Ma, H.; Zhou, Y.; Ma, L.; Zhao, S.; Shi, S.; Li, J.; Chang, Y. Gas-Sensing Properties and Mechanisms of 3D Networks Composed of ZnO Tetrapod Micro-Nano Structures at Room Temperature. *Materials* **2024**, *17*, 203. [[CrossRef](#)] [[PubMed](#)]
126. Dong, J.; Shao, J.; Sun, C.; Pan, G.; Yang, X. Preparation of Pt/WO<sub>3</sub>@ZnO hollow spheres for low-temperature and high-efficiency detection of triethylamine. *Dalton Trans.* **2024**, *53*, 3224–3235. [[CrossRef](#)] [[PubMed](#)]
127. Xie, R.; Lu, J.; Liu, Y. Carbon monoxide gas sensing properties of SnO<sub>2</sub> modified metal-organic skeleton derived NiO. *Sens. Actuators A Phys.* **2024**, *367*, 115038. [[CrossRef](#)]
128. Liu, M.; Song, P.; Zhao, B.; Ding, Y.; Yan, M. Construction of CuO nanoparticles decorated In<sub>2</sub>O<sub>3</sub> hierarchical structure for ultrasensitive and rapid trace detection formaldehyde at low temperature. *Sens. Actuators B Chem.* **2024**, *404*, 135276. [[CrossRef](#)]
129. Yang, Z.; Zhang, Z.; Mu, Y.; Yue, C.; Liu, Z.; Dastan, D.; Yin, X.; Ma, X. Improvement of gas sensitivity to ethanol by hydrothermal preparation of Dy-doped In<sub>2</sub>O<sub>3</sub>. *Sens. Actuators B Chem.* **2024**, *405*, 135386. [[CrossRef](#)]
130. Zhang, S.; Zhang, M.; Guo, Y. Highly Sensitive Ethanol Gas Sensor Based on Ag Nanoparticles Decorated In<sub>2</sub>O<sub>3</sub>. *Chem. Res. Chin. Univ.* **2024**, *40*, 1–8. [[CrossRef](#)]
131. Liu, M.; Wang, Q.; Song, P. In situ synthesis of Zn-doped In<sub>2</sub>S<sub>3</sub>/In<sub>2</sub>O<sub>3</sub> composites for the monitoring of trace ethanol at low temperature. *Vacuum* **2024**, *222*, 112956. [[CrossRef](#)]
132. Bu, W.; Liu, N.; Zhang, Y.; Han, W.; Chuai, X.; Zhou, Z.; Hu, C.; Lu, G. Atomically dispersed Pt on MOF-derived In<sub>2</sub>O<sub>3</sub> for chemiresistive formaldehyde gas sensing. *Sens. Actuators B Chem.* **2024**, *404*, 135260. [[CrossRef](#)]
133. Wang, N.; Liu, Z.; Zhou, Y.; Zhao, L.; Kou, X.; Wang, T.; Wang, Y.; Sun, P.; Lu, G. Imparting Chemiresistor with Humidity-Independent Sensitivity toward Trace-Level Formaldehyde via Substitutional Doping Platinum Single Atom. *Small* **2024**, *Early View*. [[CrossRef](#)]

**Disclaimer/Publisher's Note:** The statements, opinions and data contained in all publications are solely those of the individual author(s) and contributor(s) and not of MDPI and/or the editor(s). MDPI and/or the editor(s) disclaim responsibility for any injury to people or property resulting from any ideas, methods, instructions or products referred to in the content.